

**PL-TR-95-2105**

## **CALIBRATION OF LOCAL MAGNITUDE SCALES FOR USE IN SEISMIC MONITORING**

**J. R. Murphy  
M. E. Marshall  
B. W. Barker**

**T. J. Bennett  
L. T. Grant  
I. N. Gupta**

**Maxwell Laboratories, Incorporated  
S-CUBED Division  
P.O. Box 1620  
La Jolla, CA 92038-1620**

**August 1995**

**DTIC QUALITY INSPECTED 4**

**Final Report  
July 1994-July 1995**

**19960212 201**

**Approved for public release; distribution unlimited**



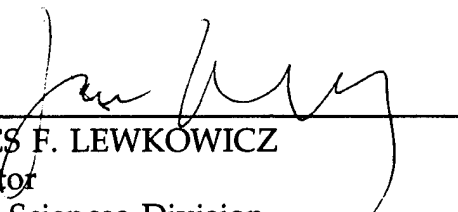
**PHILLIPS LABORATORY  
Directorate of Geophysics  
AIR FORCE MATERIEL COMMAND  
HANSCOM AFB, MA 01731-3010**

"This technical report has been reviewed and is approved for publication."



---

JAMES F. LEWKOWICZ  
Contract Manager



---

JAMES F. LEWKOWICZ  
Director  
Earth Sciences Division

This report has been reviewed by the ESD Public Affairs Office (PA) and is releasable to the National Technical Information Service (NTIS).

Qualified requestors may obtain additional copies from the Defense Technical Information Center. All others should apply to the National Technical Information Service.

If your address has changed, or if you wish to be removed from the mailing list, or if the addressee is no longer employed by your organization, please notify PL/IM, 29 Randolph Road, Hanscom AFB, MA 01731-3010. This will assist us in maintaining a current mailing list.

Do not return copies of this report unless contractual obligations or notices on a specific document requires that it be returned.

REPORT DOCUMENTATION PAGE			Form Approved OMB No. 0704-0188	
Public reporting burden for this collection of information is estimated to average 1 hour per response, including the time for reviewing instructions, searching existing data sources, gathering and maintaining the data needed, and completing and reviewing the collection of information. Send comments regarding this burden estimate or any other aspect of this collection of information, including suggestions for reducing this burden, to Washington Headquarters Services, Directorate for Information Operations and Reports, 1215 Jefferson Davis Highway, Suite 1204, Arlington, VA 22202-4302, and to the Office of Management and Budget, Paperwork Reduction Project (0704-0188), Washington, DC 20503.				
1. AGENCY USE ONLY (Leave blank)		2. REPORT DATE August 1995	3. REPORT TYPE AND DATES COVERED Final July 1994-July 1995	
4. TITLE AND SUBTITLE CALIBRATION OF LOCAL MAGNITUDE SCALES FOR USE IN SEISMIC MONITORING			5. FUNDING NUMBERS Contract: F19628-91-C-0186  PE 61102F PR 2309  TA G2 WU BL	
6. AUTHOR(S) J. R. Murphy, M. E. Marshall, B. W. Barker, T. J. Bennett, L. T. Grant*, I. N. Gupta*				
7. PERFORMING ORGANIZATION NAME(S) AND ADDRESS(ES) Maxwell Laboratories, Inc. S-CUBED Division P.O. Box 1620 La Jolla, CA 92038-1620			8. PERFORMING ORGANIZATION REPORT NUMBER  SSS-DTR-95-15147	
9. SPONSORING/MONITORING AGENCY NAME(S) AND ADDRESS(ES) Phillips Laboratory 29 Randolph Road Hanscom AFB, MA 01731-3010  Contract Manager: James F. Lewkowicz/GPE			10. SPONSORING/MONITORING AGENCY REPORT NUMBER  PL-TR-95-2105	
11. SUPPLEMENTARY NOTES  * Multimax, Inc., Landover, Maryland				
12a. DISTRIBUTION/AVAILABILITY STATEMENT  Approved for public release; distribution unlimited			12b. DISTRIBUTION CODE	
13. ABSTRACT (Maximum 200 words)  In situations where cavity decoupling of underground nuclear explosions is a plausible evasion scenario, comprehensive seismic monitoring of any eventual CTBT will require the routine identification of many small seismic events with magnitudes in the range $2.0 < m_b < 3.5$ . However, since such events are not expected to be detected teleseismically, their magnitudes will have to be estimated from regional recordings using seismic phases and frequency bands which are different from those employed in the teleseismic $m_b$ scale which is generally used to specify monitoring capability. Therefore, it is necessary to establish the $m_b$ equivalences of any selected regional magnitude measures in order to estimate the expected detection statistics and thresholds of proposed CTBT seismic monitoring networks. In the investigations summarized in this report, this has been accomplished through analyses of synthetic data obtained by theoretically scaling observed regional seismic data recorded in Scandinavia and Central Asia from various tamped nuclear tests to obtain estimates of the corresponding seismic signals to be expected from small cavity decoupled nuclear tests at those same source locations.				
14. SUBJECT TERMS Magnitude Explosion Seismic CTBT Regional Nuclear Monitoring			15. NUMBER OF PAGES 58	
			16. PRICE CODE	
17. SECURITY CLASSIFICATION OF REPORT  Unclassified	18. SECURITY CLASSIFICATION OF THIS PAGE  Unclassified	19. SECURITY CLASSIFICATION OF ABSTRACT  Unclassified	20. LIMITATION OF ABSTRACT  Unlimited	

## Table of Contents

1.0	Introduction .....	1
2.0	Magnitude Determinations For Small Seismic Events.....	2
2.1	$m_b$ Versus Yield For Underground Nuclear Explosions.....	2
2.2	$M_L$ and Other Regional Magnitude Scales.....	5
2.3	Local Magnitude Determination in the Prototype International Monitoring System (IMS) .....	7
2.4	Calibration of Regional Magnitude Scales.....	10
3.0	Simulation Analysis of Regional Magnitude Determination For Small Cavity Decoupled Underground Nuclear Explosions.....	12
3.1	Description of the Source Scaling Model.....	12
3.2	Comparison of Magnitude Estimates Determined From Synthetic Regional Waveform Data.....	16
3.3	Preliminary Evaluation of Alternate Magnitude Measures.....	34
4.0	Summary and Conclusions .....	39
4.1	Summary.....	39
4.2	Conclusions.....	41
	References.....	43

## List of Illustrations

FIGURE		PAGE
1	Comparison of $m_b$ /yield relations for underground nuclear explosions illustrating the effects of test site tectonic environment and cavity decoupling.....	4
2	Comparisons of $L_g$ magnitudes (top) and regional P-coda magnitudes (bottom) determined at NORSAR with teleseismic $m_b$ for Novaya Zemlya nuclear explosion tests (after Ringdal and Fyen, 1991). ....	11
3	Schematic diagram illustrating potential biases associated with extrapolating empirical $M_L/m_b$ relations to low magnitudes.....	13
4	Frequency dependent source scaling operators used to theoretically scale observed regional recordings from the Soviet JVE to simulate the signals expected from various cavity decoupling scenarios.....	15
5	Comparison of observed SALMON and scaled STERLING seismograms, radial component, $R = 16$ km. ....	17
6	Locations of stations (O) and events ( $\square$ ) used in the regional magnitude studies.....	19
7	Synthetic cavity decoupled regional seismograms obtained by applying the theoretical source scaling operators of Figure 4 to the IRIS station GARM ( $\Delta = 1380$ km) recording of the Soviet JVE.....	20
8	Synthetic cavity decoupled regional seismograms obtained by applying the theoretical source scaling operators to the ARCESS ( $\Delta = 1110$ km) recording of the Novaya Zemlya explosion of 10/24/90.....	21

9	Synthetic cavity decoupled regional seismograms obtained by applying the theoretical source scaling operators to the NORESS ( $\Delta = 1565$ km) recording of the Soviet PNE of 7/18/85.....	22
10	Synthetic cavity decoupled regional seismograms obtained by applying the theoretical source scaling operators of Figure 4 to the IRIS station ARU ( $\Delta = 1530$ km) recording of the Soviet JVE.....	23
11	Synthetic cavity decoupled regional seismograms obtained by applying the theoretical source scaling operators of Figure 4 to the IRIS station WMQ ( $\Delta = 950$ km) recording of the Soviet JVE.....	24
12	Synthetic cavity decoupled regional seismograms obtained by applying the theoretical source scaling operators to the IRIS station GARM ( $\Delta = 1590$ km) recording of the Lop Nor explosion of 8/16/90.....	25
13	Regional seismic magnitudes as functions of $m_b$ derived from source scaled versions of the ARCESS recording of the Novaya Zemlya nuclear explosion of 10/24/90. ....	27
14	Comparison of regional phase magnitudes estimated for two underground nuclear explosions with $m_b = 3.0$ using data recorded over different propagation paths to the ARCESS and NORESS array stations.....	28
15	Comparison of individual regional phase magnitude estimated from mine blast data recorded at ranges of 800-1200 km from the ARCESS and NORESS array stations.....	30
16	Comparison of regional phase magnitudes estimated for underground nuclear explosion with $m_b = 3.0$ using data recorded over selected Central Asia propagation paths. ....	31
17	Comparison of regional phase magnitudes determined from the IRIS station GARM recordings ( $\Delta \approx 1600$ km) of the Lop Nor nuclear explosion of 8/16/90 and an earthquake (11/03/90) located within 100 km of the Lop Nor test site...	33

18	Comparison of the frequency dependent variability of the $P_n$ , $P_g$ , $S_n$ and $L_g$ regional phase magnitudes for the selected data sample, $m_b = 3.0$ . ....	35
19	Standard deviation of the individual phase magnitudes as a function of frequency.....	37
20	Average background noise levels as a function of frequency for the five selected regional stations. ....	38
21	Modified estimates of the standard deviation of the individual phase magnitudes as a function of frequency. ....	40

## 1. INTRODUCTION

A central issue in current discussions of the seismic monitoring capability required to adequately verify any eventual Comprehensive Test Ban Treaty (CTBT) concerns the definition of the threshold level of seismic event size or magnitude down to which seismic events will have to be detected and identified. It is generally agreed that the capability currently exists to unambiguously identify almost all seismic events having magnitudes characteristic of well-coupled underground nuclear explosions with yields greater than a few kilotons (i.e.,  $m_b \sim 4$ , OTA (1988)). However, in the context of monitoring a CTBT, consideration has to be given to the requirement to characterize the much smaller signals which would be expected to result from various evasive testing practices which might be employed by a nation pursuing a clandestine nuclear weapons development program. For example, since it has been experimentally demonstrated that it is possible to reduce the amplitude of the radiated seismic signal of an underground nuclear explosion by at least a factor of 70 by employing the cavity decoupling evasion scenario, it follows that comprehensive monitoring of underground nuclear tests in the 1 to 10 kt range will necessarily involve identification analyses of small seismic events with magnitudes in the range  $2.0 < m_b < 3.5$ . However, since such small events are generally not recorded teleseismically, their magnitudes are typically determined using one of the many proposed regional magnitude scales ( $M_L$ ). This constitutes a problem in that such regional magnitude measures are defined in terms of seismic phases and frequency bands which are different from those associated with the traditional teleseismic  $m_b$  magnitude measure; and, consequently, it is not always clear how they relate to the corresponding  $m_b$  values which are used to specify seismic monitoring capability. The objective of the research program described in this report has been to attempt to develop an improved quantitative understanding of the relationship between  $M_L$  and  $m_b$  for small underground nuclear tests. This has been accomplished through analyses of synthetic data obtained by theoretically scaling observed regional seismic data recorded from tamped underground nuclear tests to obtain estimates of the corresponding seismic signals to be expected from small cavity decoupled nuclear tests at those same source locations.



This report presents a summary of the research investigations which have been conducted during the project in an attempt to define improved means for calibrating regional magnitude scales for use in seismic monitoring. The problem of magnitude determination for small seismic events is reviewed in Section 2 where the magnitude ranges of potential interest in the seismic monitoring of underground nuclear testing are assessed and various proposed regional magnitude measures are described and compared. This is followed in Section 3 by the presentation of a detailed magnitude estimation analysis which is conducted using theoretically scaled regional seismic data corresponding to those to be expected from small cavity decoupled nuclear tests conducted at various locations near Scandinavia and in Central Asia. The report concludes with Section 4 which contains a summary and statement of conclusions regarding the current state of understanding with respect to magnitude determinations for small underground nuclear explosions.

## **2. MAGNITUDE DETERMINATIONS FOR SMALL SEISMIC EVENTS**

### **2.1 $m_b$ Versus Yield For Underground Nuclear Explosions**

The seismic monitoring of underground nuclear testing is greatly complicated by the fact that the seismic measure of source size is a magnitude, which is determined from the amplitudes of the recorded seismic signals using empirically determined algorithms, whereas it is the explosive energy release or yield which is of primary interest for treaty monitoring and intelligence purposes. Consequently, much research has been conducted over the past 30 years in attempts to quantitatively relate various magnitude measures to explosion yield. For a variety of technical and historical reasons, most of this research has focused on the teleseismic  $m_b$  body wave magnitude measure; and, as a result, seismic monitoring capability is typically described in terms of detection and identification thresholds which are expressed in  $m_b$  units. However, it has long been recognized that a given  $m_b$  value may correspond to a rather wide range of possible yield values depending on the explosive source conditions and the characteristics of the propagation paths from the source area to the stations of the

monitoring network. These dependencies are schematically illustrated in Figure 1, where approximate  $m_b$ /yield curves corresponding to different testing conditions are compared. In this case, the upper reference curve labeled "Good Coupling/Stable Region" corresponds to the  $m_b$ /yield relation

$$m_b = 4.45 + 0.75 \log W \quad (1)$$

which is associated with tamped explosions at nominal containment depths in hardrock at test locations in stable continental interior regions, such as the former Soviet Semipalatinsk test site. The corresponding "Good Coupling/Tectonic Region" curve shown in this figure was obtained from (1) by subtracting 0.40 units  $m_b$  to account for upper mantle attenuation bias such as that observed between NTS and Semipalatinsk. The curves labeled "Low Coupling" in this figure are meant to be representative of explosions in dry porous media such as the dry alluvium and tuff media at NTS and are offset below the corresponding reference hardrock curves by 0.75 units  $m_b$ . Finally, the curves labeled "Cavity Decoupled" are shown offset below the reference hardrock curves by 1.85 units  $m_b$  (i.e. the logarithm of the nominal full decoupling factor of 70). Thus, 1 kt fully decoupled nuclear tests at normal containment depths in stable and tectonic regions are expected to correspond on average to  $m_b$  values of 2.6 and 2.2, respectively. Similarly, 10 kt fully decoupled explosions in stable and tectonic regions are expected to correspond to  $m_b$  values of 3.35 and 2.95, respectively. As a further specific point of reference, 1 kt and 10 kt fully decoupled explosions in good coupling media at NTS would be expected to correspond on average to  $m_b$  values of about 2.1 and 2.9, respectively. Further variations of several tenths of a magnitude unit from these average values may be expected for cavity decoupled tests conducted in different media, or at depths significantly different from the nominal containment depths for tamped explosions with comparable yields.

In any case, it follows from the above discussion that comprehensive monitoring of underground nuclear testing in the 1 to 10 kt range will necessarily involve analyses of small seismic events with magnitudes in the range  $2.0 < m_b < 3.5$ , at least in regions where cavity decoupling is considered to be feasible over this yield range. Of course, such events will not be detected teleseismically; and, while it is possible to estimate the equivalent  $m_b$  ranges using first order

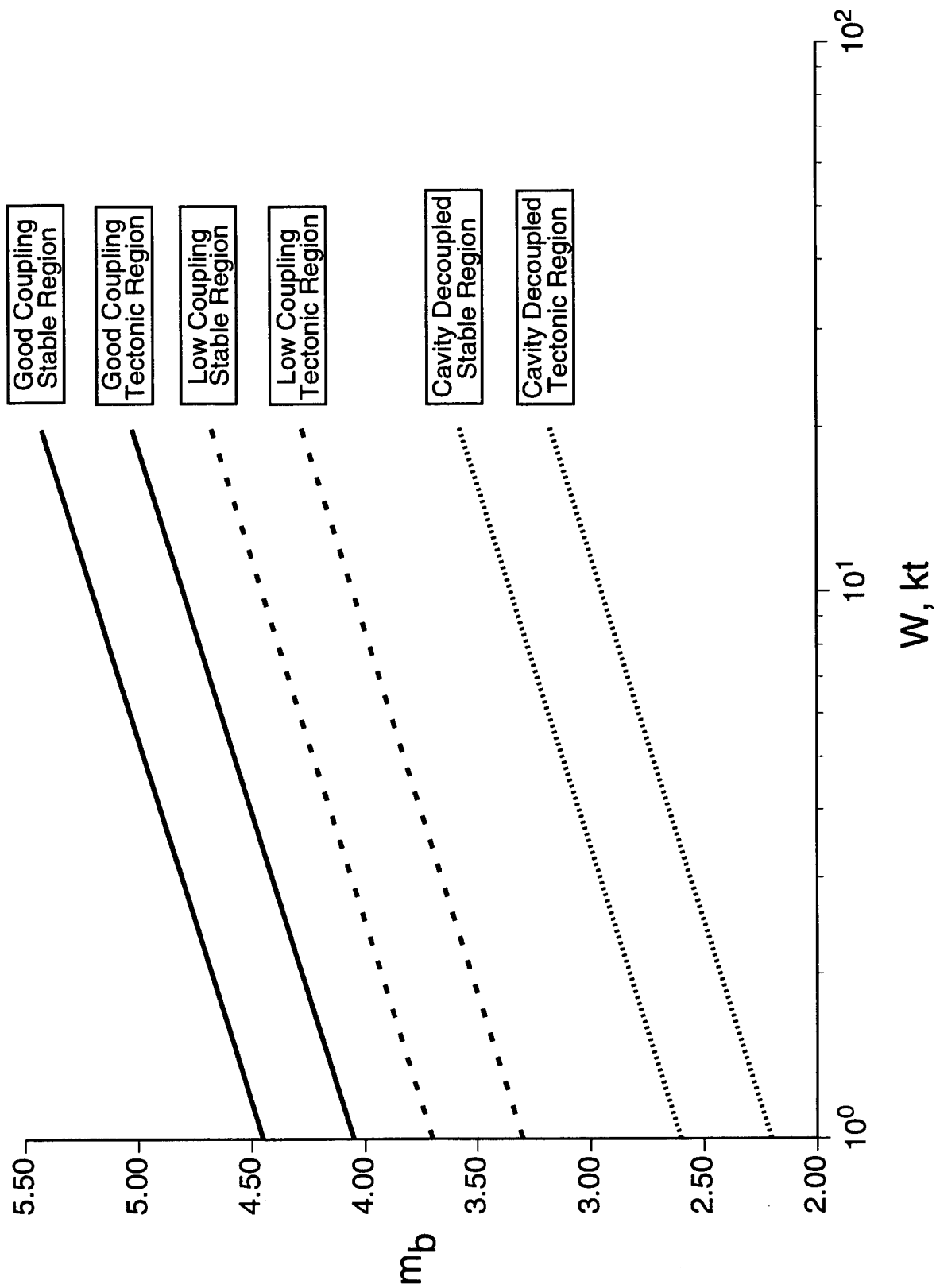


Figure 1. Comparison of  $m_b$ /yield relations for underground nuclear explosions illustrating the effects of test site tectonic environment and cavity decoupling.

analytical models, measured  $m_b$  values will not be available for such explosions. That is, the magnitudes of these events will have to be determined from seismic data observed at regional distances using one or more of the proposed local magnitude algorithms. However, since these magnitudes are generally estimated using seismic phases and frequency bands which are different from those employed in the teleseismic  $m_b$  scale, it is often not clear how they relate to  $m_b$ , particularly for small events for which no direct calibration data are available. This uncertainty has significant implications with respect to seismic monitoring, because ultimately the analysis threshold for bulletin preparation will have to be expressed in terms of a local magnitude. It follows that it is important to establish a firm, quantitative understanding of the relationship between  $m_b$  and selected local magnitude measures for small, cavity decoupled nuclear explosions of monitoring concern.

## **2.2 $M_L$ and Other Regional Magnitude Scales**

The magnitude scale originally defined by Richter (1935) was intended to measure the relative sizes of seismic events in southern California recorded by stations equipped with a standard seismograph system (viz Wood-Anderson). The Richter magnitude scale, like most of the  $M_L$  magnitude scales which have followed, was basically a short-period measure of the maximum trace amplitude with a correction for attenuation. Gutenberg (1945a,b) made the magnitude scale more generally applicable by introducing the surface-wave magnitude,  $M_S$ , and body-wave magnitude,  $m_b$ , based on teleseismic measurements. These  $m_b$  and  $M_S$  scales have traditionally been the most widely used for measuring the sizes of teleseismic events. Although it was originally intended that the different magnitude scales should provide a consistent measure of source strength, it is recognized today that this is not the case. Among the reasons for such differences in the magnitude measures are variations in path attenuation from the nominal corrections, excitation differences related to depth, source geology, and mechanism, and differences in station site response and recording instruments. In principle, adjustments could be made to account for these differences, but the required information is not always available and simplifying assumptions are often made.

The magnitude problem is further complicated by the proliferation of regional stations and station networks over the past two decades. In many areas the seismic events recorded by these regional stations are small, and they may not be recorded by stations outside the region. In such situations magnitude calibration may be difficult and ad hoc procedures, similar to those originally applied by Richter, are often used to establish a local magnitude scale.

One of the most widely used magnitude scales for use with regional stations is the  $m_b(L_g)$  scale developed by Nuttli (1973). This scale is based on a measure of the amplitude of the high-frequency regional  $L_g$  phase and is corrected for propagation effects using an attenuation model which is specific to each region. However, variations also exist in the techniques used for the  $m_b(L_g)$  scale which again may produce inconsistency in comparison to other magnitude measures. Variations in the frequency passband of the signal, window selection and amplitude measurement procedure (e.g., RMS versus peak), and attenuation differences and radiation pattern (especially for small numbers of stations) can all alter the  $m_b(L_g)$  measurement and complicate its interpretation in terms of source strength.

As a result of installation of the ARPA regional arrays in Fennoscandia and Central Europe, the seismic monitoring thresholds in this broad region have been pushed to a very low level. Over the years several different magnitude scales have been used to describe the sizes of seismic events in the Fennoscandia region. Ringdal (1983) adapted Nuttli's  $m_b(L_g)$  magnitude technique for application to regional array digital data recorded in Norway and proposed an additional magnitude technique based on regional P coda. Sereno and Bratt (1988) applied an inversion technique to the amplitude spectra of  $P_n$  and  $L_g$  signals from Fennoscandian events recorded at NORESS and derived region-specific attenuation relations for the two phases which could be used to refine regional-phase magnitude formulae. The latter study also offered some insight into the detection capabilities of NORESS as a function of frequency and distance for specific magnitude thresholds based on the attenuation model derived from the inversion.

Båth *et al.* (1976) developed a local magnitude scale, analogous to the Richter scale, which was widely used throughout Scandinavia to define the relative sizes of small events. The Båth *et al.* local magnitude formula is:

$$M_L = \log(100 \cdot D) + F(\Delta, T) \quad (2)$$

where  $D$  is the maximum amplitude of the  $L_g$  ground motion in micrometers,  $\Delta$  is epicentral distance in km,  $T$  is the dominant period of the measured phase in seconds, and  $F(\Delta, T)$  is a correction for attenuation and shape of the instrument response curve which has been tabulated for ranges from 50 km to 1500 km and dominant periods from 0.3 sec to 1.4 sec based on observations from events around Sweden. This Båth magnitude formula was used at NORSAR originally to compute  $M_L$  from NORESS data, with the  $D$  and  $T$  being computed automatically for  $L_g$  using the RONAPP signal processing module (cf. Mykkeltveit and Bungum, 1984). The amplitude  $D$  at this time was measured as the maximum amplitude of the  $L_g$  phase from a coherent beam steered to the  $L_g$  velocity and the azimuth determined from f-k analysis and  $T$  was determined by averaging the periods of several cycles near the peak amplitude. Subsequently, the NORESS algorithm was modified to the form

$$M_L = \log(100 \cdot A) + B(\Delta, T_0) \quad (3)$$

where  $A$  is the peak  $L_g$  amplitude measured in a group velocity window between 3.0 and 3.6 km/sec from the 2-4 Hz filtered incoherent beam and  $B$  is the same as the  $F(\Delta, T)$  defined by Båth except that the correction term is at a fixed frequency of 2.2 Hz, approximating the dominant frequency of the  $L_g$ , which is also used to determine an approximate instrument response to use in correcting the trace amplitude to ground motion in micrometers.

### **2.3 Local Magnitude Determination in the Prototype International Monitoring System (IMS)**

The local magnitude algorithm which has been in use at the prototype IMS running at the ARPA Center for Monitoring Research (CMR) over the past several years is quite different from the traditional  $M_L$  measures described in the

preceding section (Bache *et al.*, 1991). In particular, it is based on measurements of the amplitudes of four distinct regional phases:  $P_n$ ,  $P_g$ ,  $S_n$  and  $L_g$ . These amplitude measurements and associated magnitude determinations are made for the array stations NORESS, ARCESS, FINESA and GERESS when those stations are at ranges of  $15^\circ$  or less from the seismic events. The phase amplitudes are measured from the incoherent beams at each array formed from the vertical component traces filtered in the 2-4 Hz frequency band. The amplitudes used for the  $M_L$  computations are based on the short-term, average (STA) amplitudes determined by averaging the incoherent beam records over 1 second time windows and are defined to be the maxima of the STA's in the 4 second windows following the automatically determined detection times for each phase.

The STA amplitudes determined from the incoherent beams are next corrected for noise using the long-term average (LTA) amplitudes determined from the average of the incoherent beam record over a long time window prior to the P phase for the event. The actual length of the LTA window appears to be station dependent but usually is on the order of 50-60 seconds. If there is no detected P phase at a station for a particular event,  $M_L$  is not measured at that station.  $M_L$  is also only used for a particular phase if the STA for that phase is at least 1.1 times as large as the LTA. So, we now have for the noise-corrected amplitude for each phase

$$\text{Amp} = (\text{STA}^2 - \text{LTA}^2)^{1/2} \quad (4)$$

The final magnitude formulae involve a correction for station distance (attenuation) and a normalization to the  $M_L$  procedures of the past, specifically those used in the previous version of the IMS processing system. The current magnitude formulae are of the form:

$$M_L(\text{phase}) = \log(\text{Amp}) + A + B \cdot \Delta + C \cdot \log(\Delta) \quad (5)$$

where  $\Delta$  is the epicentral distance in kilometers. Different attenuation relations are defined for each of the regional phases,  $P_n$ ,  $P_g$ ,  $S_n$  and  $L_g$ , as shown in Table 1. The attenuation relationships (involving the B and C coefficients) are the same for NORESS, ARCESS and FINESA but different for GERESS. Normalization terms (the A term in the  $M_L$  formula) are different for each array and are set

**Table 1: Attenuation and Normalization Terms for use in  $M_L$  Formulae for Different Regional Phases and Array Stations**

Station	Phase	A	B	C	$\sigma$
ARCESS	$P_n$	-5.942	0.0	1.9793	0.236
ARCESS	$P_g$	-3.894	0.00073674	1.0	0.221
ARCESS	$S_n$	-4.053	0.00065665	1.0934	0.115
ARCESS	$L_g$	-4.140	0.00071908	1.0	0.147
FINESA	$P_n$	-5.235	0.0	1.9793	0.236
FINESA	$P_g$	-3.095	0.00073674	1.0	0.221
FINESA	$S_n$	-3.313	0.00065665	1.0934	0.115
FINESA	$L_g$	-3.379	0.00071908	1.0	0.147
GERESS	$P_n$	-5.082	0.000394	2.052	0.393
GERESS	$P_g$	-4.247	0.000883	1.665	0.401
GERESS	$S_n$	-3.337	0.00117	1.168	0.340
GERESS	$L_g$	-7.735	0.00109	2.906	0.336
NORESS	$P_n$	-6.005	0.0	1.9793	0.236
NORESS	$P_g$	-3.773	0.00073674	1.0	0.221
NORESS	$S_n$	-4.050	0.00065665	1.0934	0.115
NORESS	$L_g$	-4.095	0.00071908	1.0	0.147

corresponding to the signal amplitude measured in digital counts (not nanometers). Thus, in this formulation the propagation path corrections to any given array are taken to be the same for any event lying within  $15^\circ$  of that array; and the associated distance attenuation corrections are taken to be the same for all such events recorded at the three Scandinavian array stations. The implications of these assumptions with respect to possible region-specific biases in the  $M_L$  determinations will be discussed further in the following sections.

The final IMS  $M_L$  value is determined from a weighted sum of all phase magnitudes using the individual phase uncertainty values ( $\sigma$ ) listed in Table 1. It can be seen that the inverse variance weighted averaging algorithm is the same for all three Scandinavian arrays and is given by

$$M_L = 0.11 M(P_n) + 0.13 M(P_g) + 0.47 M(S_n) + 0.29 M(L_g) \quad (6a)$$



while for GERESS

$$M_L = 0.21 M(P_n) + 0.21 M(P_g) + 0.29 M(S_n) + 0.29 M(L_g) \quad (6b)$$

Thus, the local magnitude determinations at the three Scandinavian arrays are heavily weighted on the  $S_n$  and  $L_g$  phases; while those at GERESS represent a more nearly even weighting of the data from the four different phases. Such differences between stations serve to illustrate the fact that calibration of multi-phase magnitude algorithms is a complex task.

## 2.4 Calibration of Regional Magnitude Scales

As was noted previously, a primary design objective of all magnitude scales implemented since the original formulation of Richter has been that they provide consistent and unbiased measures of source strength. However, because the wide variety of magnitude measures which have been proposed over the years are based on a multitude of seismic phases and encompass a range of different dominant frequencies, it has proved to be very difficult to quantitatively reconcile the various magnitude scales. That is, even after careful calibration for regional propagation path differences, the empirical nature of most magnitude measures makes it difficult to determine the absolute levels of the scales relative to some standard, such as teleseismic  $m_b$ . For calibration of regional magnitude scales, the general practice has been to assemble a sample of events which are large enough to have been recorded at both regional and teleseismic distances and to directly compare the regional and teleseismic magnitudes for such events to determine an average calibration constant. Thus, for example, Ringdal and Fyen (1991) investigated  $L_g$  and P-coda magnitudes measured at the NORSAR array from Novaya Zemlya nuclear explosion tests. Figure 2 shows comparisons of the regional magnitudes from these events with  $m_b$ 's determined from teleseismic measurements. The least-squares line fits to the data indicate close correspondence between the different magnitude measures at high magnitude levels, with  $M(L_g) \approx M(P \text{ coda}) \approx m_b$  at  $m_b = 5.8$ , where the relations are best constrained by the available data. Note, however, that the slope of the least-squares fit to these  $M(L_g)$  versus  $m_b$  data is significantly less than 1.0. In fact,

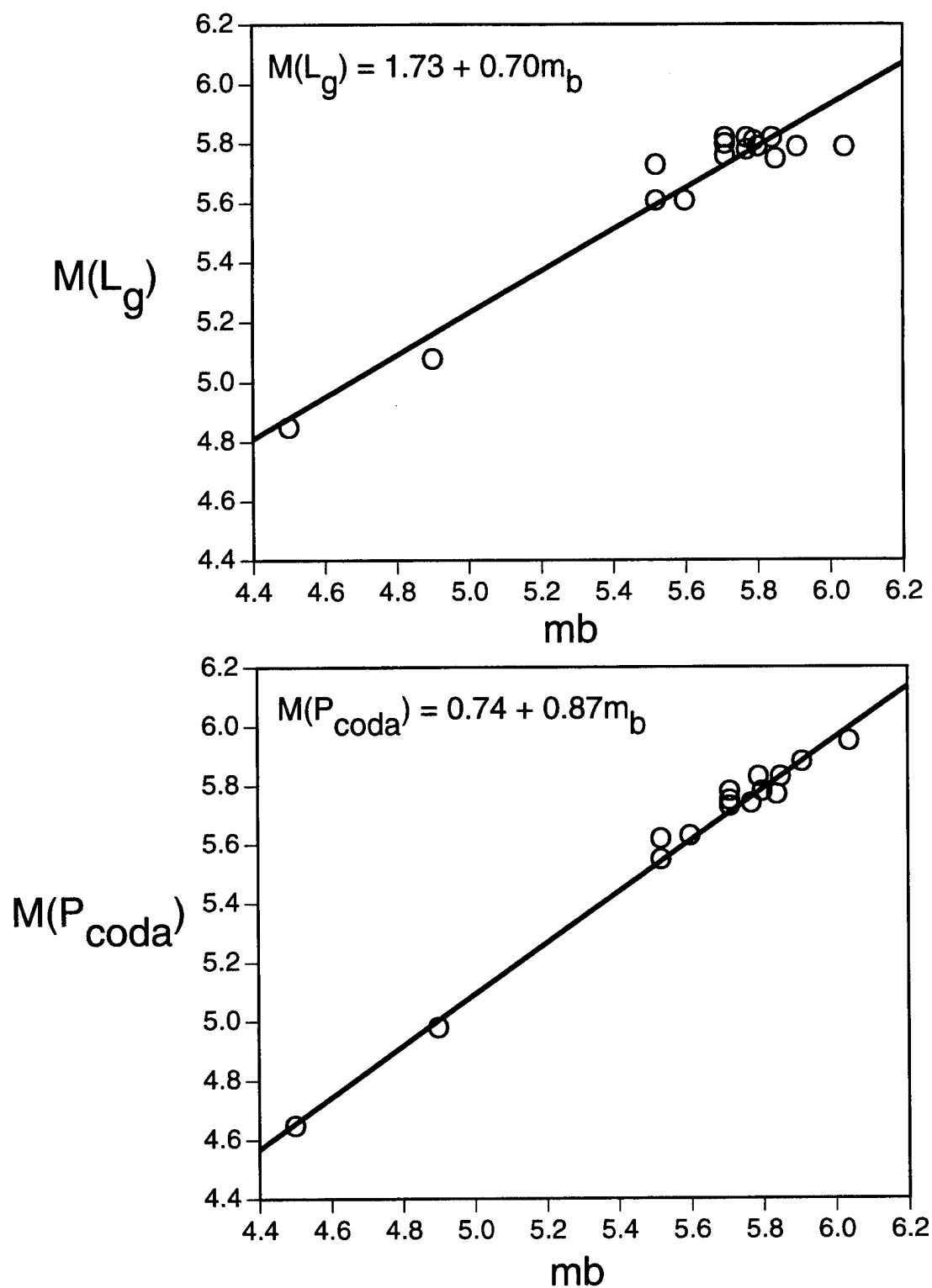


Figure 2. Comparisons of  $L_g$  magnitudes (top) and regional P-coda magnitudes (bottom) determined at NORSAR with teleseismic  $m_b$  for Novaya Zemlya nuclear explosion tests (after Ringdal and Fyen, 1991).

this fit predicts an  $M(L_g)$  value of about 4.8 for an event with  $m_b = 4.4$  and, if the same relation applies to lower magnitude levels, would predict an  $M(L_g)$  value of about 3.4 for an event with  $m_b = 2.5$ . This is obviously a major discrepancy which would have to be carefully considered in any assessments of monitoring requirements.

More generally, because such empirical magnitude calibrations are necessarily confined to events which are large enough to be well recorded teleseismically ( $m_b > 4$ ), extrapolations down into the  $m_b = 2$  range will always be subject to considerable uncertainty. This is particularly true for magnitude measures based on data representative of frequency bands significantly different from the nominal 1 Hz band usually associated with teleseismic  $m_b$ . In such cases, variations in source corner frequency effects as a function of magnitude may result in nonlinear relations between the two magnitude scales. This situation is schematically illustrated in Figure 3 for a hypothetical case in which a local magnitude measure has been calibrated to  $m_b$  using data from large events. Clearly, supplemental data and analysis procedures are required to reduce these magnitude estimation uncertainties for small seismic events.

### **3. SIMULATION ANALYSIS OF REGIONAL MAGNITUDE DETERMINATION FOR SMALL CAVITY DECOUPLED UNDERGROUND NUCLEAR EXPLOSIONS**

#### **3.1 Description of the Source Scaling Model**

An obvious means for improving calibration of regional magnitude scales for use in seismic monitoring would be to directly determine such magnitudes using data observed from small decoupled explosions of known yield. Unfortunately, however, the only such data which are known to exist consist of a few near-regional recordings from the small U.S. decoupling test STERLING and from the Soviet partial decoupling experiment conducted at Azgir in 1976. Since these data sample very restricted ranges of source and propagation path conditions, they are of limited use for magnitude calibration purposes. An alternate approach which has been pursued in the present study is to theoretically

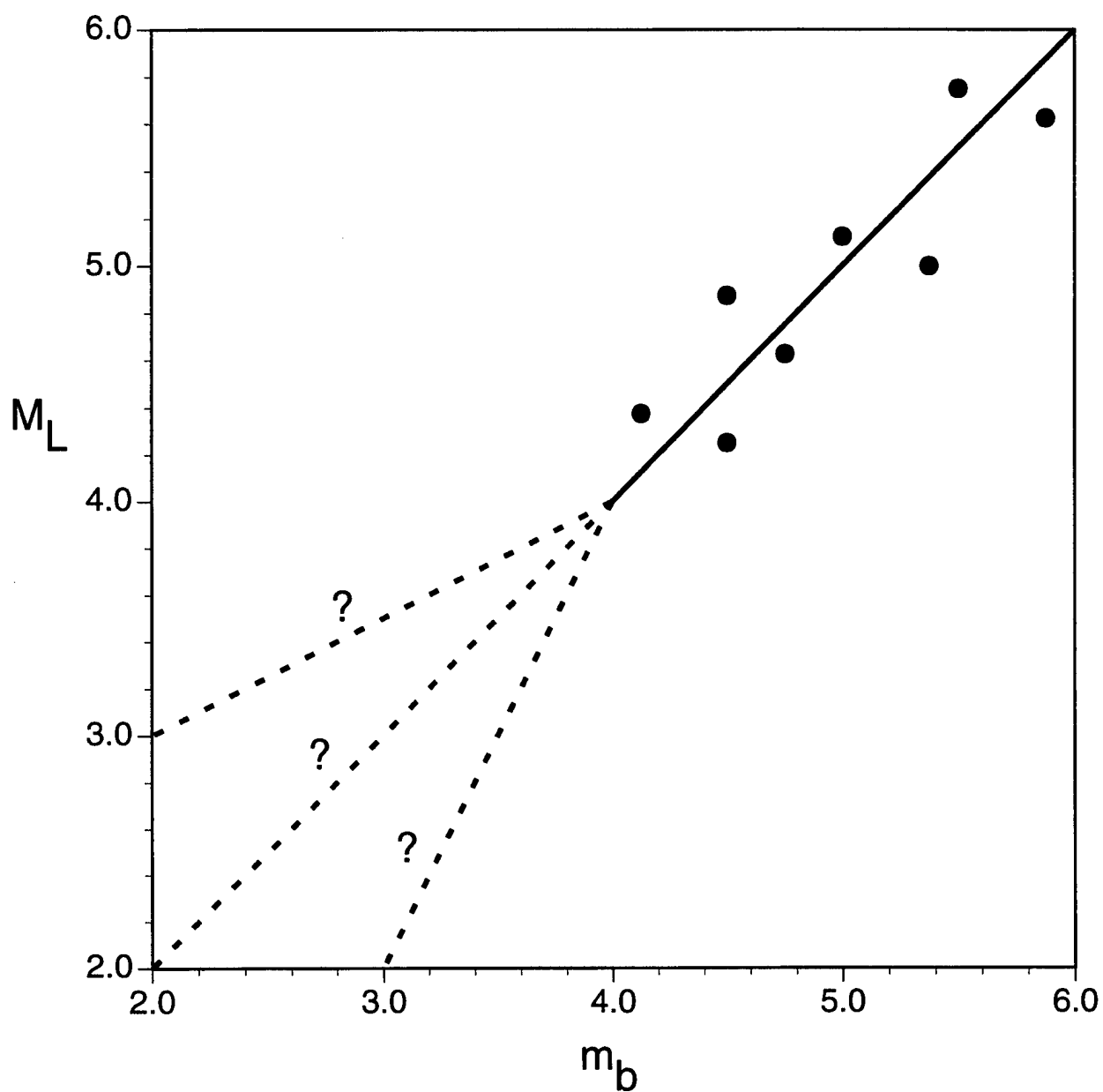


Figure 3. Schematic diagram illustrating potential biases associated with extrapolating empirical  $M_L/m_b$  relations to low magnitudes.

scale observed regional seismic data recorded from tamped underground nuclear tests to obtain estimates of the corresponding seismic signals to be expected from small cavity decoupled tests at those same source locations. Since the  $m_b$  values corresponding to such synthetic data are directly calculable, regional magnitude measures determined from these signals can be evaluated as functions of  $m_b$  down to very low thresholds, thus providing an improved basis for calibration.

The scaling procedure used to derive the synthetic regional seismic data analyzed in this study has been described in detail by Murphy and Barker (1994). In this approximation, if the elastic radius of the seismic source of the tamped reference explosion of the yield  $W_T$  is denoted as  $rel_2$ , then the elastic radius for the corresponding cavity decoupled explosion is

$$rel_1 = \frac{rel_2}{(DF)^{1/3}} \quad (7)$$

where DF denotes the decoupling factor for a particular yield/cavity volume ratio. For the purposes of the scaling exercises described in this report, values for  $rel_2$  have been assigned to each explosion using the Mueller/Murphy scaling relations for tamped explosions in granite (Mueller and Murphy, 1971). For each selected tamped explosion we have considered a range of decoupling factors which increase incrementally by factors of 2 such that  $DF = 2, 4, 8, \dots, 70 W_T$  where  $70 W_T$  corresponds to the case of 1 kt fully decoupled with a low frequency decoupling factor of 70. Now, for values of  $W_T < 100$  kt, the corner frequency of the tamped explosion source generally lies above 1 Hz and, consequently, the  $m_b$  values corresponding to such a sequence of partially decoupled synthetic explosions can be approximated simply as

$$m_{bi} = m_b(T) - \log (2, 4, 8, \dots, 70 W_T) \quad (8)$$

where  $m_b(T)$  is the observed  $m_b$  value of the tamped explosion with yield  $W_T$ . A typical sequence of such source spectrum scaling operators is shown in Figure 4 for the Soviet JVE event, where a nominal seismic yield of about 115 kt has been used for that explosion. It can be seen from this figure that the scaling is strongly frequency dependent over this regional band extending from 0.1 to 20 Hz, particularly for the operators corresponding to the lower yield decoupled

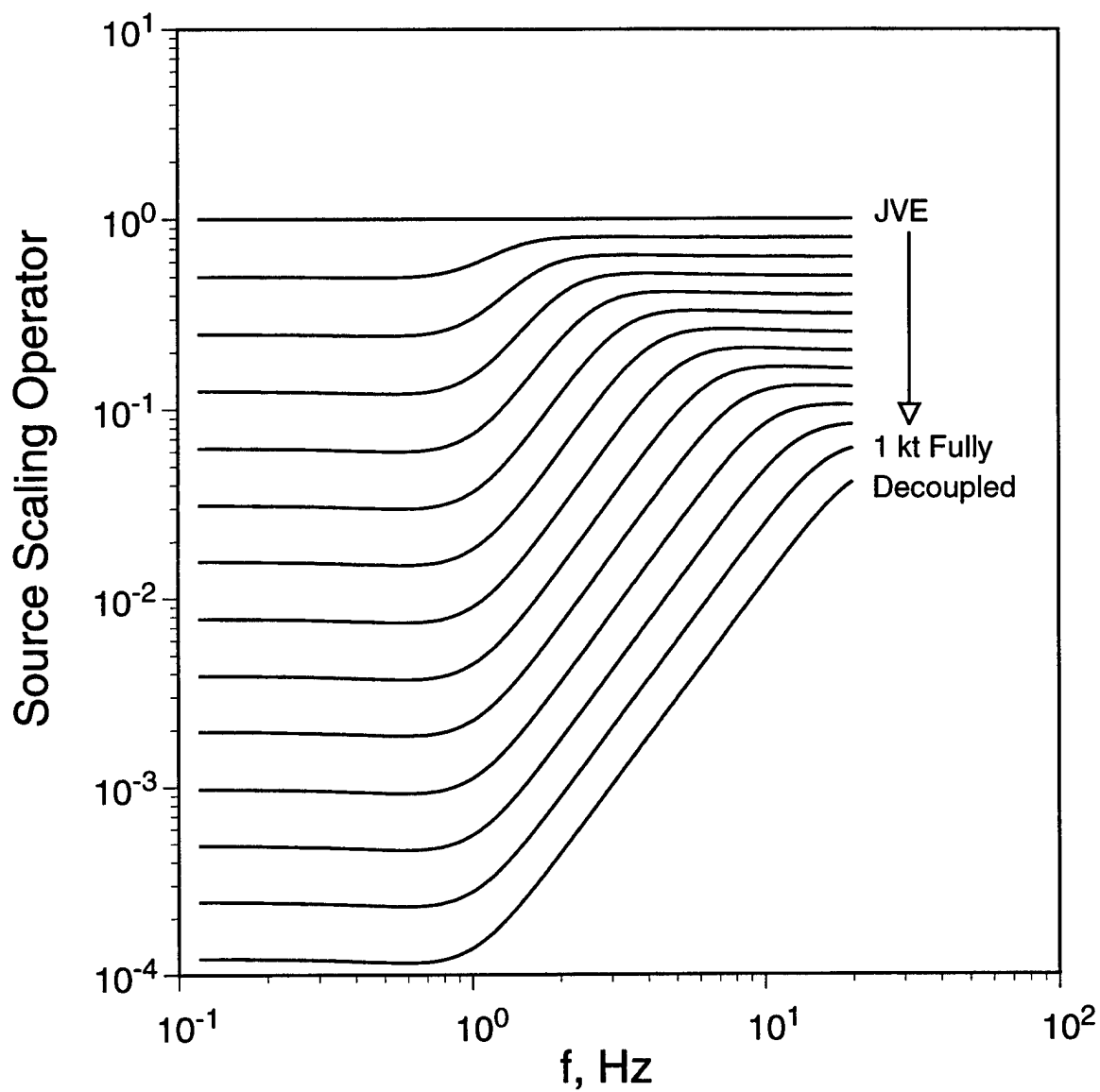


Figure 4. Frequency dependent source scaling operators used to theoretically scale observed regional recordings from the Soviet JVE to simulate the signals expected from various cavity decoupling scenarios.

explosions. It has been found that such simple approximations to the frequency dependent effects of cavity decoupling are remarkably consistent with the observed short-period data recorded from such tests (Murphy, 1977). This fact is illustrated in Figure 5, where the broadband seismic data observed from STERLING (top) at a station located 16 km from the source has been theoretically transformed into the seismic signal expected from the tamped 5.3 kt SALMON explosion at that same station (center) using a simple source spectral ratio consistent with those shown in Figure 4. Comparison of this synthetic with the corresponding observed SALMON data from that station (bottom) reveals excellent agreement with respect to amplitude level, waveform and relative spectral composition. It is concluded that the proposed source scaling model should provide useful approximations to the regional seismic signals to be expected from small, cavity decoupled nuclear explosions.

### 3.2 Comparison of Magnitude Estimates Determined From Synthetic Regional Waveform Data

The sample of tamped underground nuclear explosions for which regional seismic data were scaled using the procedures described in the preceding section are listed in Table 2. It can be seen that the selected sample represents four different test locations (i.e., Novaya Zemlya, Semipalatinsk (JVE), Lop Nor and a Soviet PNE site near Archangel at 66°N, 41°E), as well as propagation paths in

**Table 2: Tamped Explosion Data Sample**

Event		Station	Estimated Yield, kt	$\Delta$ , km
Novaya Zemlya	10/24/90	ARCESS	65	1110
PNE (Archangel)	7/18/85	NORESS	8.5	1564
Soviet JVE	9/14/88	WMQ	115	950
Soviet JVE	9/14/88	GARM	115	1380
Soviet JVE	9/14/88	ARU	115	1530
Lop Nor	8/16/90	GARM	215	1590

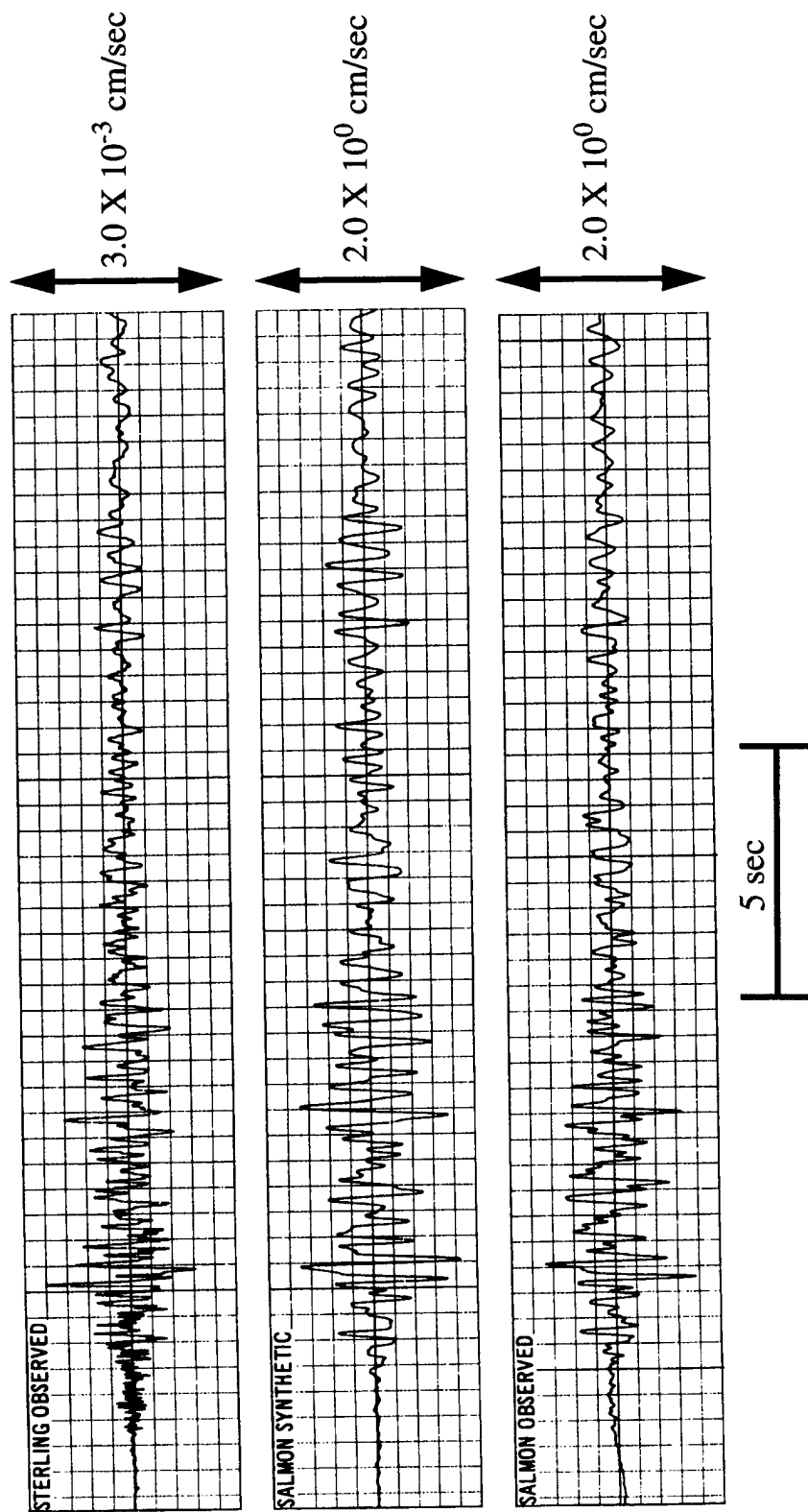


Figure 5. Comparison of observed SALMON and scaled STERLING seismograms, radial component,  $R = 16 \text{ km}$ .



Scandinavia and Central Asia over an epicentral distance range extending from about  $8.5^{\circ}$  to  $14^{\circ}$ . The map locations of these selected explosions and recording stations are shown in Figure 6. The yield values listed in this table are approximate and represent a mix of announced and inferred values which should be accurate enough for the purposes of the present investigation. Short-period, vertical-component recordings corresponding to each of the entries in Table 2 have been theoretically scaled down to a source level representative of a 1 kt fully decoupled explosion at each of these source locations using source scaling operators comparable to those shown for the JVE explosion in Figure 4. Not surprisingly, such frequency dependent scaling can have some pronounced effects on the characteristics of the corresponding broadband regional seismograms. This is illustrated in Figure 7 which shows the results of scaling the IRIS station GARM recording of the Soviet JVE ( $\Delta = 1380$  km) using the range of source scaling operators from Figure 4. It can be seen that in this case the lower frequency  $L_g$  and  $R_g$  signals are progressively attenuated with respect to the higher frequency P signals as the data are scaled to lower  $m_b$  values. Clearly, such large variations in relative phase amplitudes can be expected to have pronounced effects on at least some regional magnitude measures. Similar scaling results for the other five source/station pairs of Table 2 are shown in Figures 8-12. Note that in all of these scaling exercises, the noise has been scaled along with the signal, so that these data are not directly applicable to assessments of variations of signal-to-noise ratios with decreasing magnitude. This representation is convenient for the purposes of the present study in that it allows us to analyze the magnitude calibration issues without having to simultaneously consider the complicating effects of frequency dependent noise. The influence of background noise on magnitude determination for small events will be addressed in a later section in conjunction with an assessment of the relative utility of various alternate regional magnitude measures.

Regional magnitudes have been determined for each of the sequence of synthetic seismograms shown in Figures 7-12 using the IMS algorithm described in Section 2.3. That is, the synthetic data have been bandpass filtered in the 2-4 Hz band; and the maximum amplitudes in 4 second windows following the expected onset times of the  $P_n$ ,  $P_g$ ,  $S_n$  and  $L_g$  phases have been measured. Note from Figures 7-12 that there are a number of cases where there are no obvious arrivals at the marked group arrival times, especially for  $P_g$ . In a fully automatic

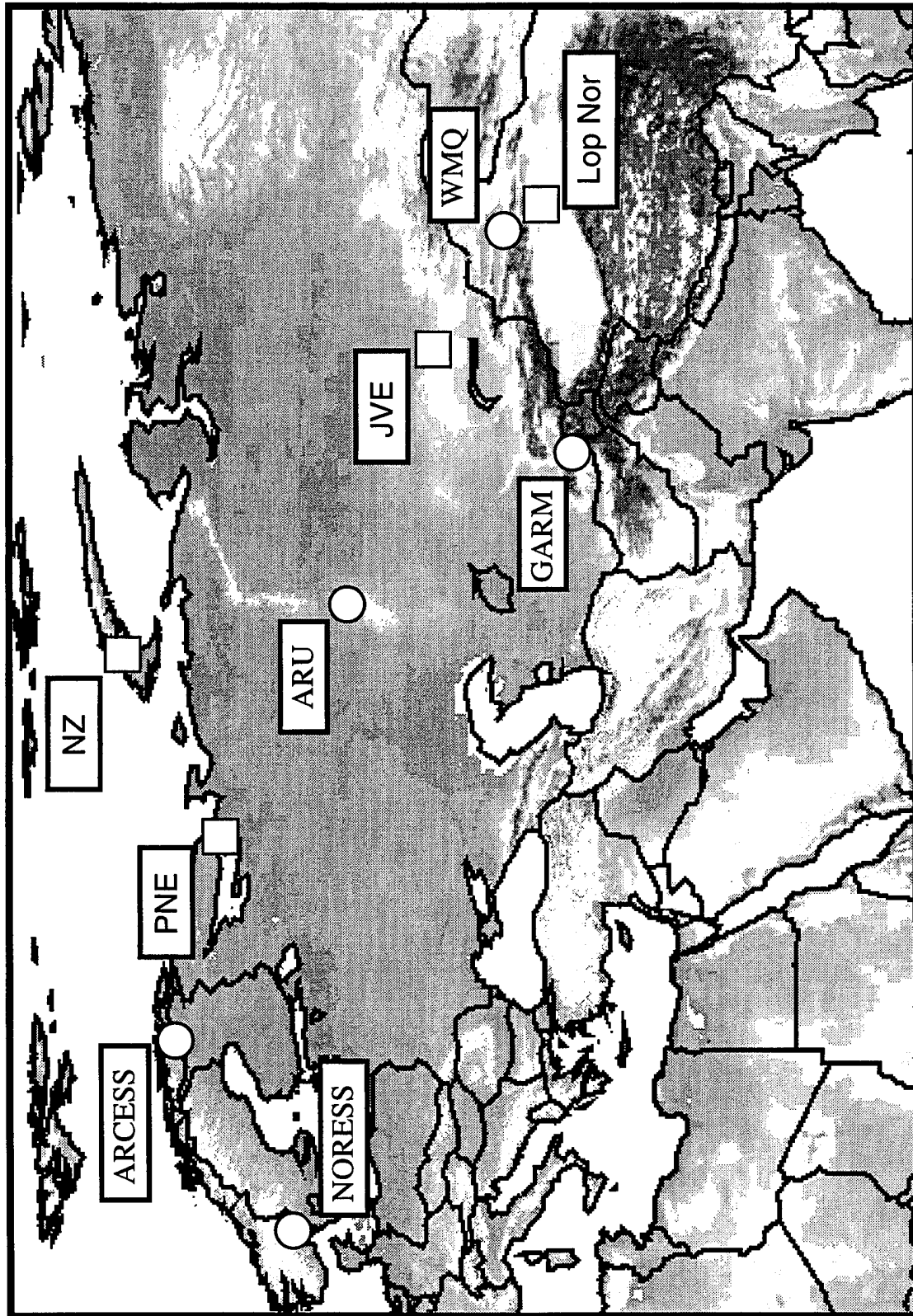


Figure 6. Locations of stations (○) and events (□) used in the regional magnitude studies.

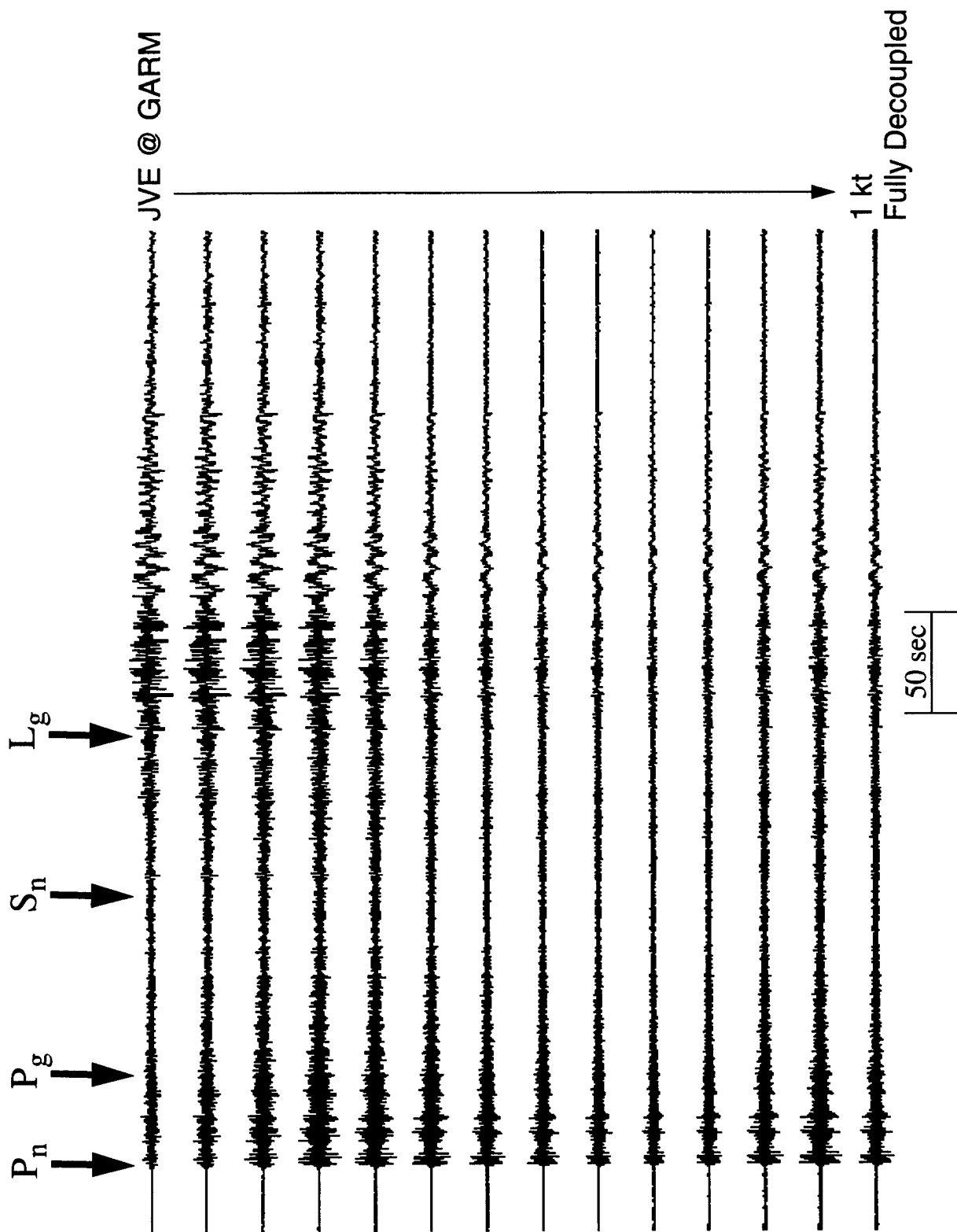


Figure 7. Synthetic cavity decoupled regional seismograms obtained by applying the theoretical source scaling operators of Figure 4 to the IRIS station GARM ( $\Delta = 1380$  km) recording of the Soviet JVE.

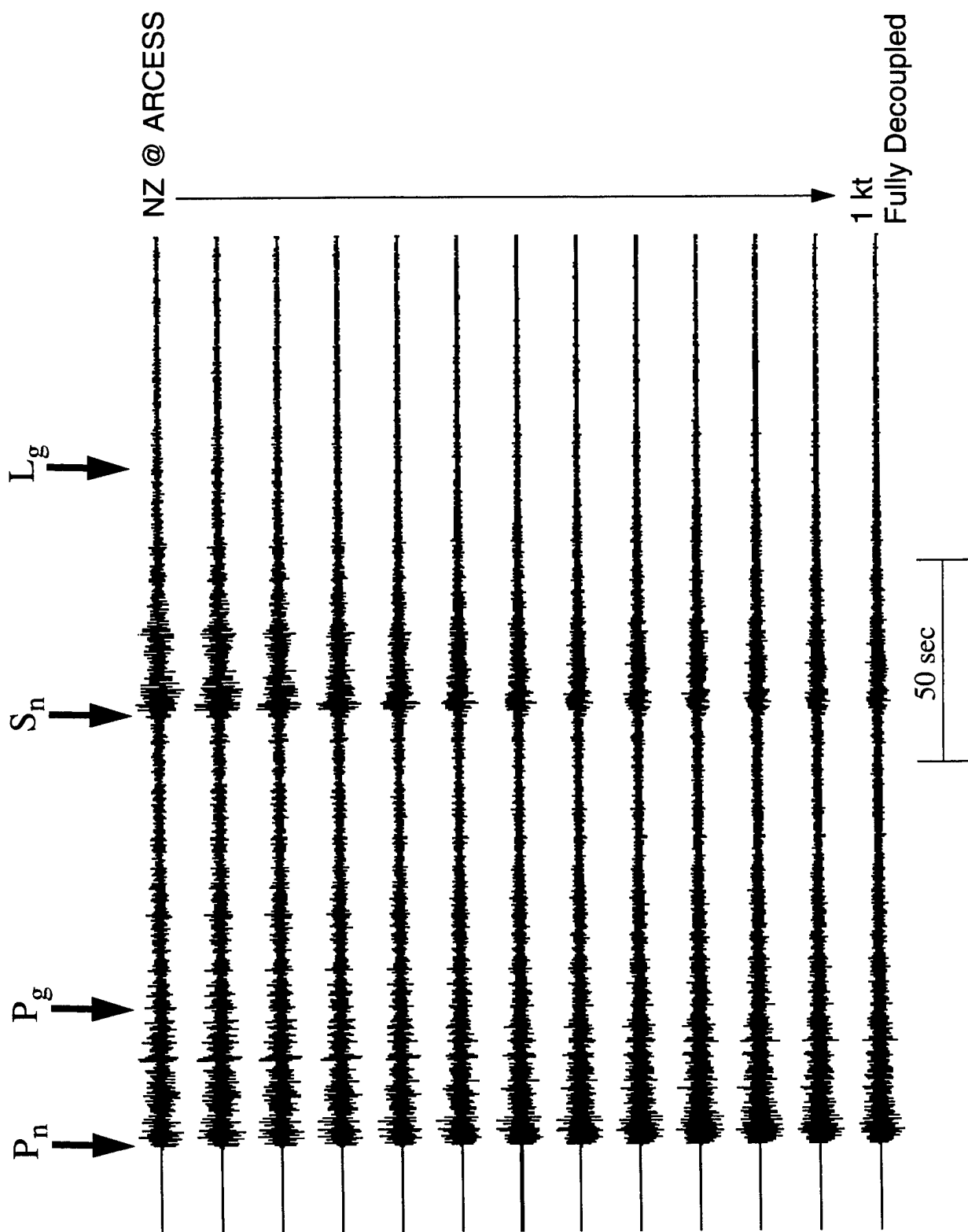


Figure 8. Synthetic cavity decoupled regional seismograms obtained by applying the theoretical source scaling operators to the ARCESS ( $\Delta = 1110$  km) recording of the Novaya Zemlya explosion of 10/24/90.

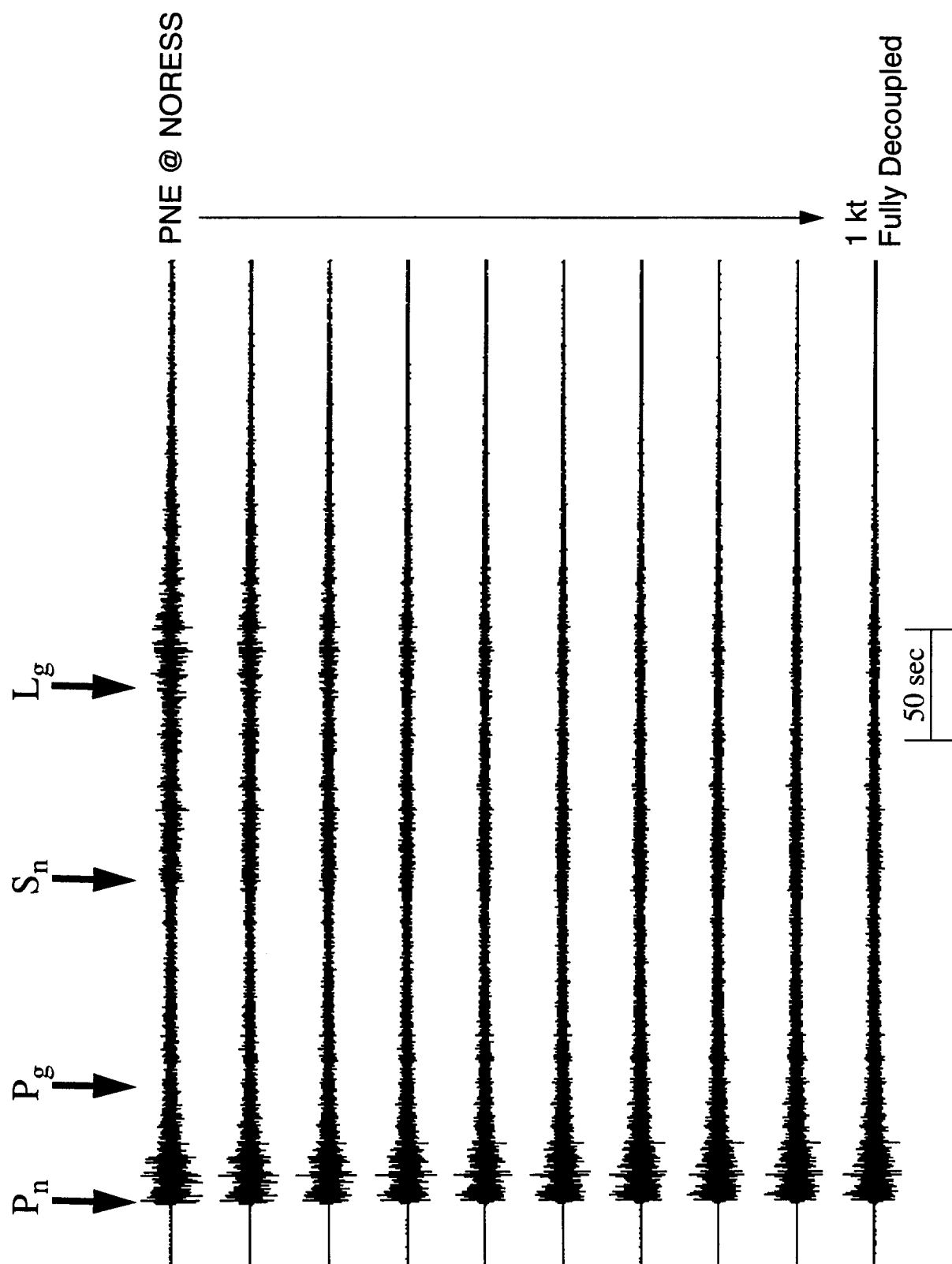


Figure 9. Synthetic cavity decoupled regional seismograms obtained by applying the theoretical source scaling operators to the NORESS ( $\Delta = 1565$  km) recording of the Soviet PNE of 7/18/85.

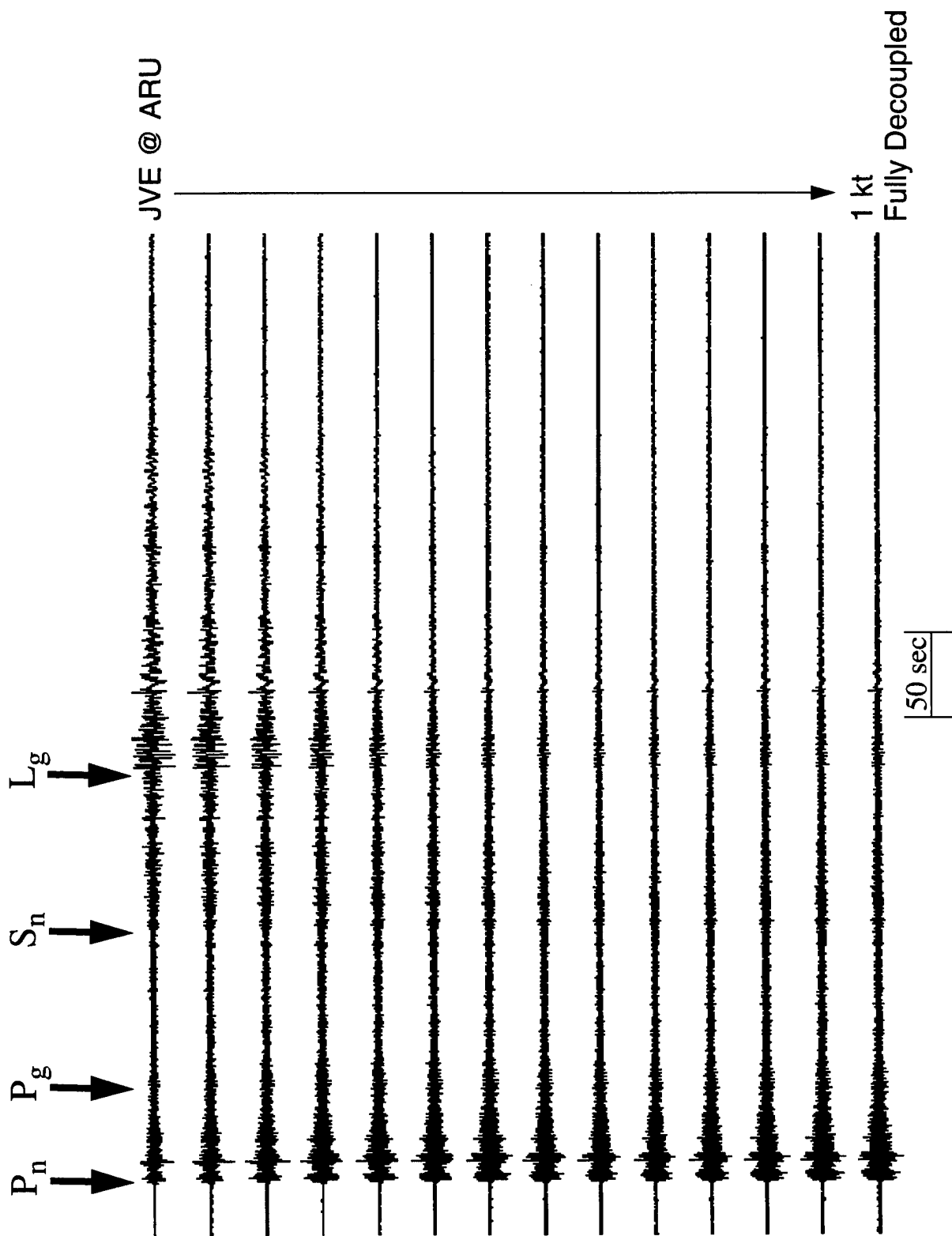


Figure 10. Synthetic cavity decoupled regional seismograms obtained by applying the theoretical source scaling operators of Figure 4 to the IRIS station ARU ( $\Delta = 1530$  km) recording of the Soviet JVE.

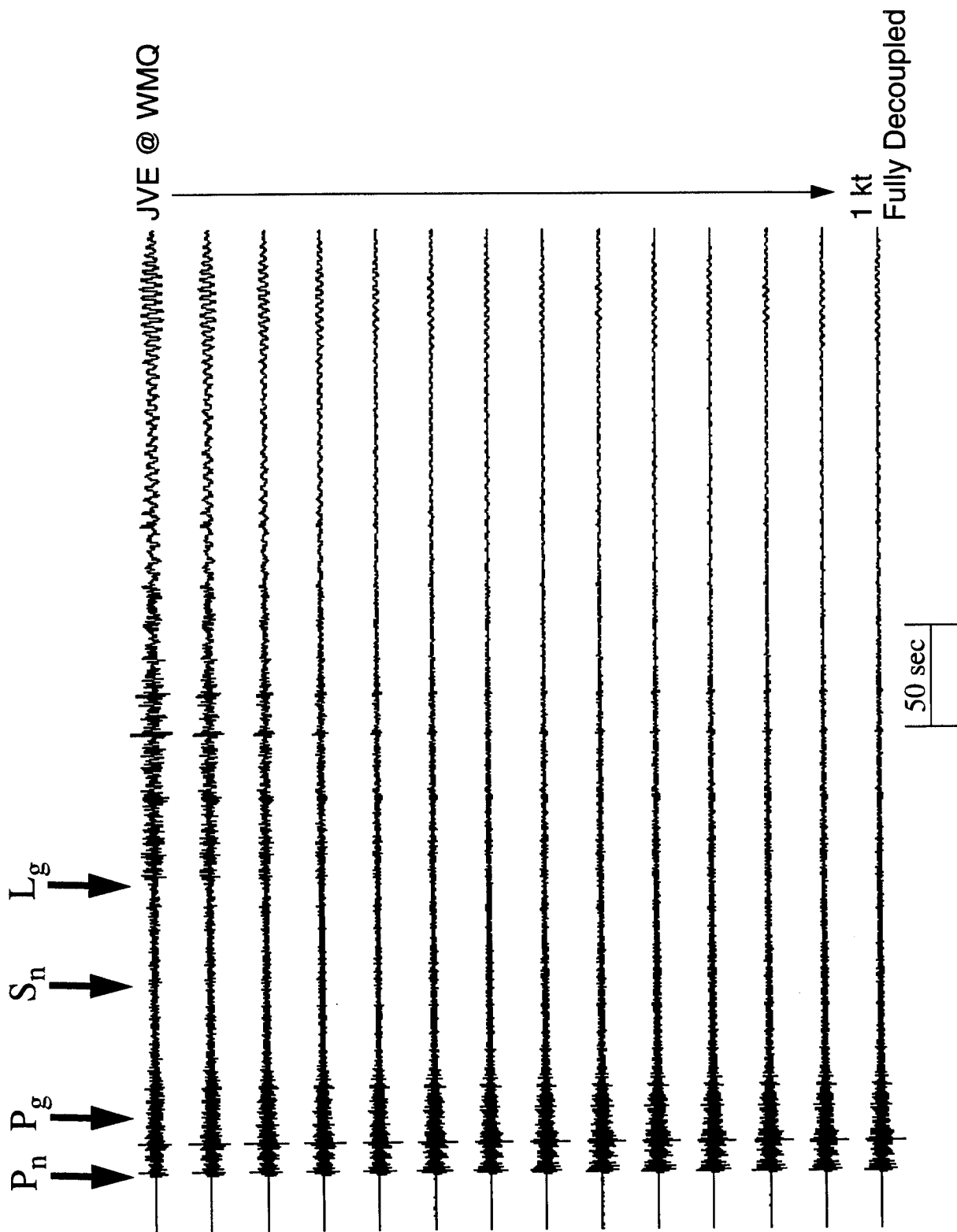


Figure 11. Synthetic cavity decoupled regional seismograms obtained by applying the theoretical source scaling operators of Figure 4 to the station WMQ ( $\Delta = 950$  km) recording of the Soviet JVE.

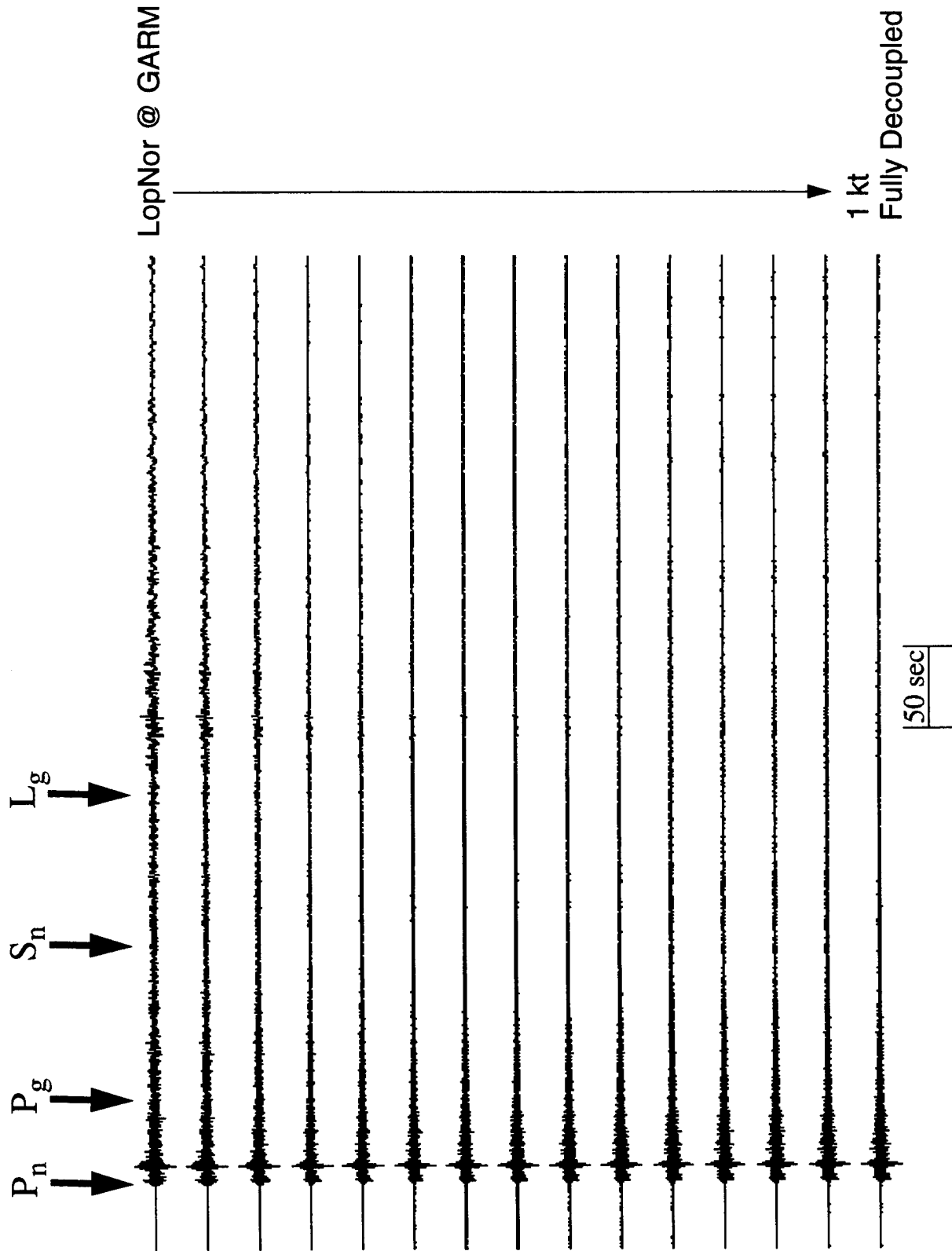


Figure 12. Synthetic cavity decoupled regional seismograms obtained by applying the theoretical source scaling operators to the IRIS station GARM ( $\Delta = 1590$  km) recording of the Lop Nor explosion of 8/16/90.



system such as the prototype IMS, it is unlikely that there would be phase detections at some of these designated times; and, consequently, no corresponding phase magnitudes would be determined by the system. However, for the purposes of the present analysis, all four phase amplitudes were measured in every case on the basis of the nominal expected group arrival times.

The individual phase magnitudes determined from the sequence of seismograms derived from the ARCESS recording of the Novaya Zemlya explosion of 10/24/90 (cf. Figure 8) are plotted versus  $m_b$  in Figure 13, where the corresponding  $M_L = m_b$  relations are also shown as solid lines for reference purposes. It can be seen that there is some curvature in the  $M_L$  versus  $m_b$  relations for the larger events, which is associated with the translation of the decoupled source function corner frequency through the selected 2-4 Hz passband as the decoupling effectiveness increases. However, the inferred relations between  $M_L$  and  $m_b$  all become linear at the low magnitude levels of principal interest, where they can be directly compared with the ideal linear relation. It can be seen from this figure that the individual phase magnitudes for this explosion show some significant departures from the expected  $M_L = m_b$  relations, with the  $P_n$  and  $S_n$  values biased high by about 0.6 magnitude units and the  $L_g$  values biased low by about 0.4 magnitude units for the smaller events. This broad scatter is presumably due to the fact that the phase propagation paths from Novaya Zemlya to ARCESS are quite different from those of the regional earthquakes and mine blasts which were used to calibrate the ARCESS magnitude determination algorithm. Such variability in propagation path effects can be illustrated by a direct comparison of this Novaya Zemlya explosion recording at ARCESS (Figure 8) with the PNE explosion at NORESS (Figure 9). Note the dramatic differences in relative phase excitation (e.g.,  $S_n/L_g$ ) for these two propagation paths located within  $15^\circ$  of these Scandinavian array stations.

The implications of these differences with respect to magnitude determination are illustrated more clearly in Figure 14 where the individual phase and weighted average magnitudes are compared for the scaled Novaya Zemlya and PNE recordings corresponding to  $m_b = 3.0$ . It can be seen that, except for the  $L_g$  magnitude, the estimated magnitudes for the PNE event are all close to the expected value of 3.0, which reflects the fact that these data were recorded from a well calibrated path. The Novaya Zemlya values on the other

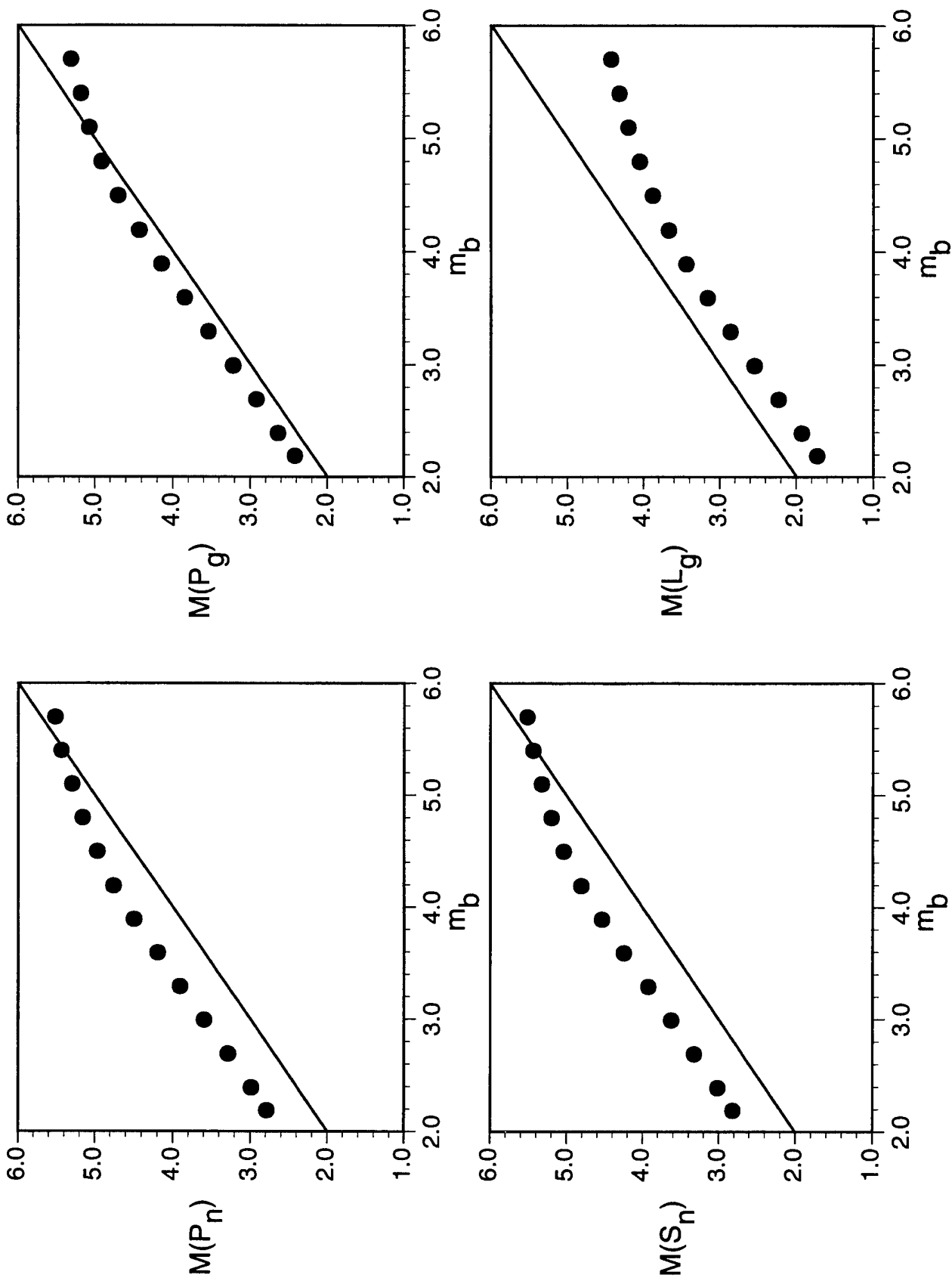


Figure 13. Regional seismic magnitudes as functions of  $m_b$  derived from source scaled versions of the ARCESS recording of the Novaya Zemlya nuclear explosion of 10/24/90.

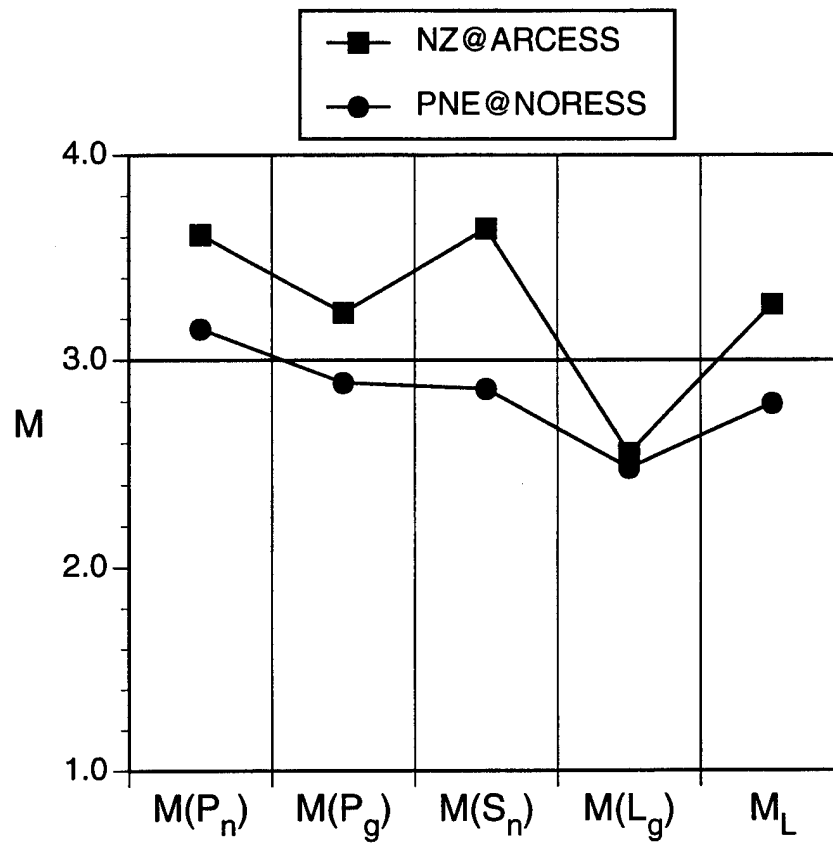


Figure 14. Comparison of regional phase magnitudes estimated for two underground nuclear explosions with  $m_b = 3.0$  using data recorded over different propagation paths to the ARCESS and NORESS array stations.

hand are widely scattered, consistent with the differences in relative phase amplitudes noted above. This example dramatically illustrates the fact that, even for very extensively calibrated stations like ARCESS, significant biases can occur for events occurring in locations which are not represented in the calibration database.

Another notable anomaly illustrated by Figure 14 is the tendency for the explosion  $L_g$  magnitudes to be lower than those determined from the other phases. This has been found to be a consistent result of the study, even for well-calibrated propagation paths, and it seems likely that this apparent bias is due to systematic differences in relative phase excitation levels associated with the different source types. That is, since the regional magnitude determination algorithms are generally calibrated using earthquake and mine blast data, it can be expected that the  $L_g$  magnitudes will be biased low for explosion sources, due to characteristic differences in the average  $L_g/P$  amplitude ratios for these different source types. Support for this hypothesis is provided in Figure 15, which shows the individual phase magnitudes for five mine blast events recorded in the 800-1200 km distance range from ARCESS and NORESS, normalized to an average P wave magnitude of 3.0. It can be seen that for these sources, the  $L_g$  magnitudes are comparable to those determined from the other phases, unlike the nuclear explosion results of Figure 14. An interesting consequence of these differences in relative phase excitation is that, even after extensive calibration with earthquake and mine blast sources, regional magnitude determinations for nuclear explosions will be lower than the corresponding  $m_b$  values, at least in those cases in which  $L_g$  data are used. It follows that if a decision is made to monitor to an  $m_b$  threshold corresponding to a particular cavity decoupling evasion scenario, it will be necessary to analyze events down to a somewhat lower regional magnitude threshold which will depend on the specific details of the regional magnitude algorithm employed.

The regional phase magnitudes determined from the scaled Central Asian recordings of the Soviet JVE explosion and the Chinese Lop Nor explosion of 8/16/90 corresponding to  $m_b = 3.0$  are displayed in Figure 16, where it can be seen that the individual values vary by as much as two full magnitude units for this selected sample of data. In these examples, the individual phase magnitudes were again estimated using the Scandinavian propagation algorithms in order to

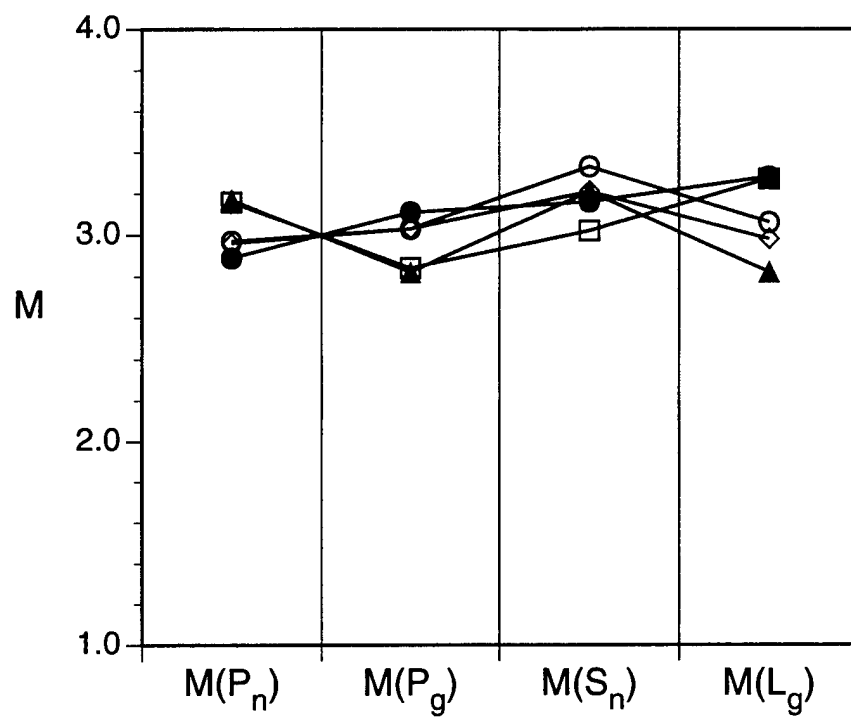


Figure 15. Comparison of individual regional phase magnitude estimated from mine blast data recorded at ranges of 800-1200 km from the ARCESS and NORESS array stations.

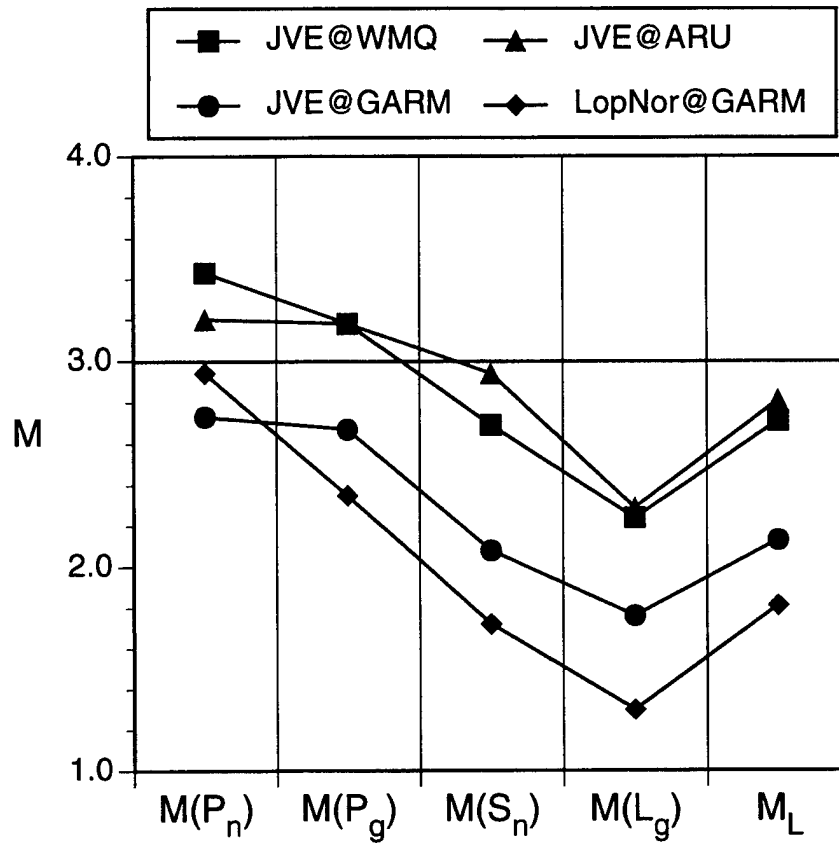


Figure 16. Comparison of regional phase magnitudes estimated for underground nuclear explosion with  $m_b = 3.0$  using data recorded over selected Central Asia propagation paths.

provide a constant reference base for comparison purposes. Consequently, it could be expected that careful path calibration studies for these specific paths would result in a significant reduction in the variability displayed here. However, these results do serve to dramatically emphasize the very strong dependence of regional phase characteristics on the properties of the propagation paths. It follows that the addition of new stations to a regional monitoring network will generally necessitate the collection and detailed analysis of large representative calibration databases for each station before these stations can be expected to contribute meaningful data for use in the determination of regional magnitudes.

It can also be seen from Figure 16 that the  $L_g$  magnitudes determined from these Central Asian recordings show the same tendency to be low relative to the other phase magnitudes which was noted previously for the Scandinavian explosions of Figure 14. In this case, of course, the lack of path specific propagation corrections is no doubt contributing to some extent to this large observed offset. However, as with the Scandinavian data, it appears that characteristic source differences are also playing a role in this case. Thus, for example, Figure 17 shows a comparison of the regional phase magnitudes (normalized to an average P wave magnitude of 4.0) determined from the IRIS station GARM recordings of the Lop Nor explosion of 8/16/90 and an earthquake (11/03/90) located within 100 km of the Lop Nor test site. In this case, it can be seen that there are significant differences in the relative regional phase magnitudes for these two source types recorded over a nearly common propagation path, with the earthquake showing evidence of much larger S/P and  $L_g$ /P amplitude ratios than the explosion in this selected 2-4 Hz frequency band. The differences in this case are even larger than those found in the corresponding Scandinavian comparisons (cf. Figures 14 and 15). This may reflect the fact that the  $L_g$ /P excitation differences between earthquakes and nuclear explosions are larger than those between the mine blasts and nuclear explosions used in the Scandinavian comparisons. In any case, this Central Asian example is consistent with the Scandinavian results in that it indicates that regional magnitude algorithms which are calibrated using earthquake and mine blast data will not be directly applicable to nuclear explosion data.

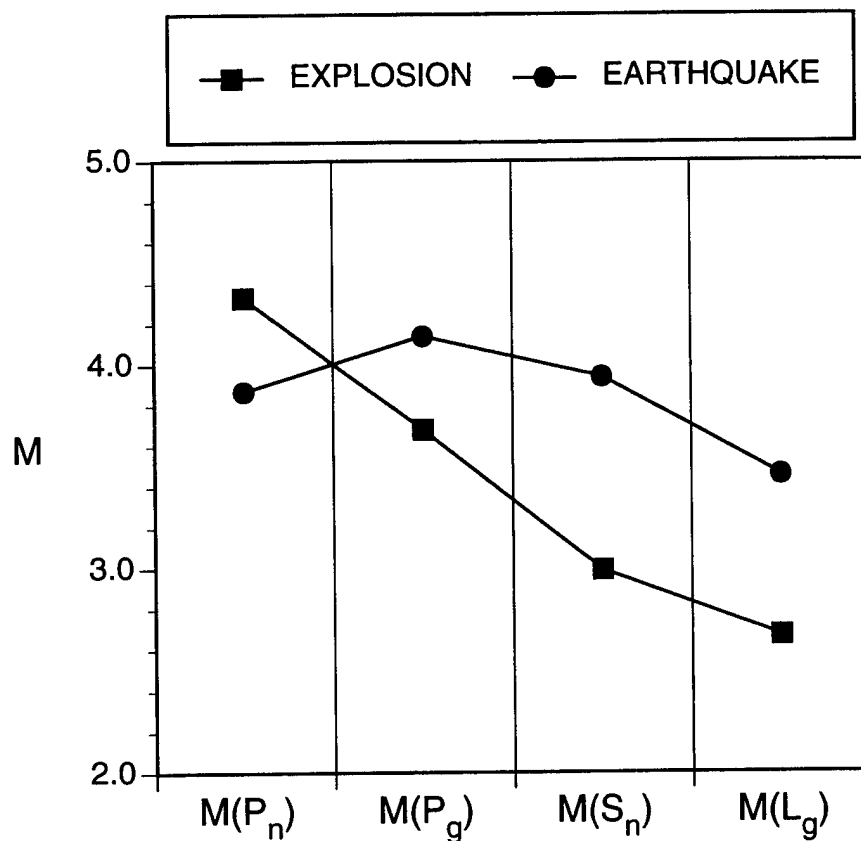


Figure 17. Comparison of regional phase magnitudes determined from the IRIS station GARM recordings ( $\Delta \approx 1600$  km) of the Lop Nor nuclear explosion of 8/16/90 and an earthquake (11/03/90) located within 100 km of the Lop Nor test site.



### 3.3 Preliminary Evaluation of Alternate Magnitude Measures

The analyses presented above have focused exclusively on the prototype IMS regional magnitude algorithm developed for the ARPA array stations. That is, they have been limited to consideration of a single magnitude measure based on a particular weighted average of four regional phase amplitudes (i.e.,  $P_n$ ,  $P_g$ ,  $S_n$  and  $L_g$ ) measured from seismic recordings filtered in the 2-4 Hz passband. It is natural to question, therefore, whether there might not be other phase weightings or frequency bands which would provide more nearly optimal measures of source size for use in seismic monitoring. In general, this is a complex question, particularly in the context of implementation in an automatic system which must perform reliably over a wide range of operating conditions. For such applications, issues related to frequency dependent noise variability and calibration complexity can play important roles in the algorithm selection process. In the following preliminary analysis, a number of these factors will be considered separately in an attempt to illustrate their relative importance with respect to regional magnitude determination.

Considering first the effects of frequency, Figure 18 shows a comparison of the frequency dependent variations of the four selected phase magnitudes over the band extending from about 1 to 6 Hz, as determined from data recorded from the selected nuclear explosions, scaled to a common value of  $m_b = 3.0$ . In these examples, the Scandinavian propagation corrections for the nominal 2-4 Hz band (plotted at a center frequency of about 3 Hz in Figure 18) were applied in all cases; and, consequently, these results are far from optimal for the different frequency bands and propagation paths. However, they do provide a clear picture of the relative difficulty of the magnitude calibration problem as a function of these variables. Thus, for example, it can be seen that the variability generally increases with increasing frequency, which suggests that high frequency magnitude estimates will be quite sensitive to the accuracy of the inferred propagation path corrections for the different regions of interest. Furthermore, it can be seen from Figure 18 that the observed variability for the  $S_n$  magnitude measure is generally larger than those for the other phase magnitudes, particularly at the higher frequencies. This may reflect the well-documented strong dependence of  $S_n$  amplitudes on regional variations in upper mantle velocity and attenuation characteristics.

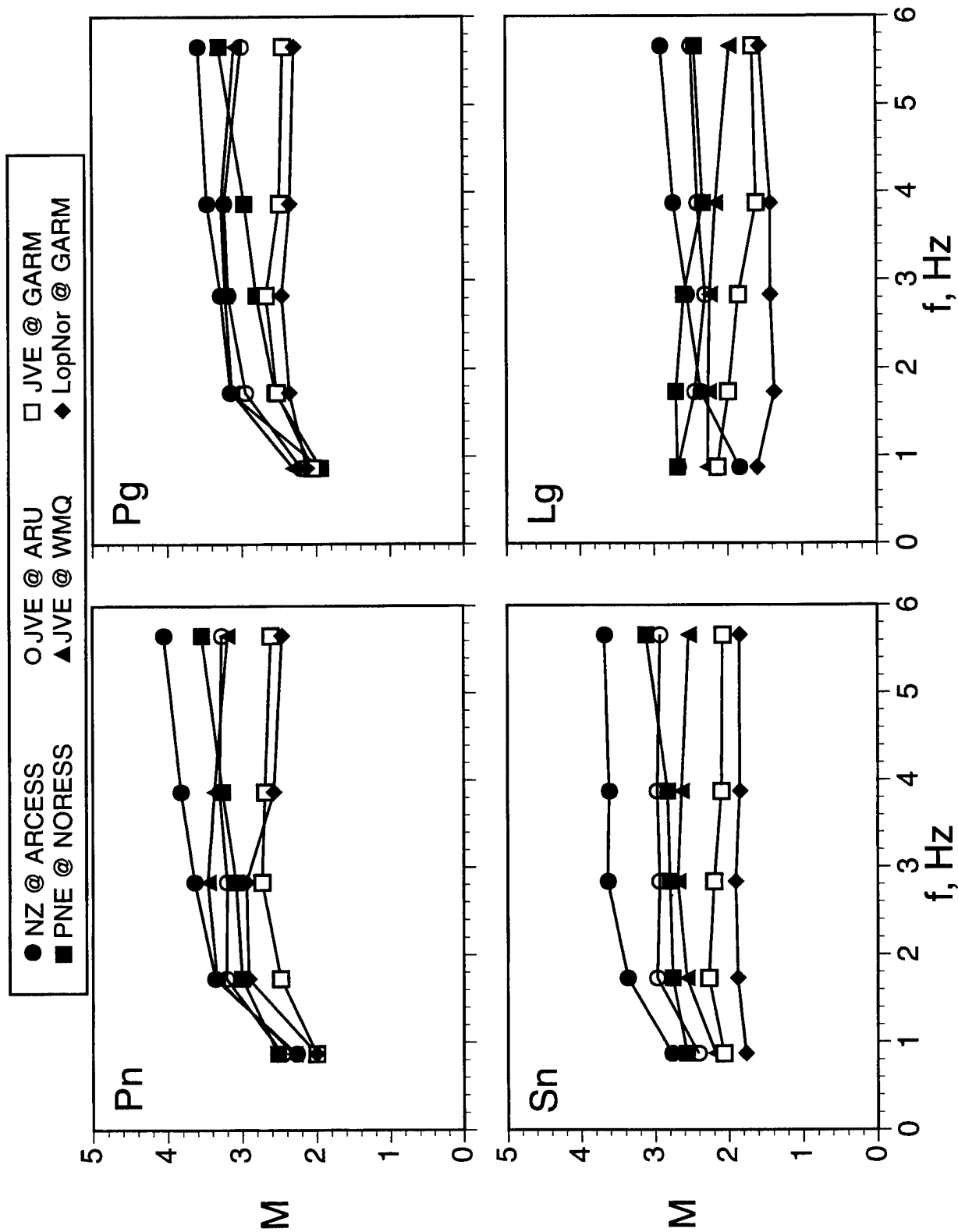


Figure 18. Comparison of the frequency dependent variability of the  $P_n$ ,  $P_g$ ,  $S_n$  and  $L_g$  regional phase magnitudes for the selected data sample,  $m_b = 3.0$ .

This dependence of observed variability on regional phase type and frequency is illustrated more clearly in Figure 19 where the standard deviation ( $\sigma_M$ ) of the individual phase magnitude determinations from Figure 18 are plotted as a function of frequency for each phase. It can be seen that  $\sigma_M$  increases with increasing frequency for all four phases, and achieves a minimum value of about 0.14 at a frequency of about 1 Hz for the  $P_g$  phase. This is somewhat ironic in that, as was noted previously in conjunction with the discussions of Figures 7-12,  $P_g$  is often not a distinct phase in these data; and  $M(P_g)$  often simply represents a P coda measurement. In any case, a straightforward interpretation of these results would seem to suggest that low frequency P wave data might provide the basis for a more stable regional magnitude measure than that provided by the IMS algorithm. However, while there might be some merit to this suggestion for well-recorded, larger events, it ignores the fact that the noise background is strongly frequency dependent. Thus, Figure 20 shows a comparison of average noise spectra estimated for the stations ARCESS, NORESS, ARU, GARM and WMQ which have been used in the present study. It can be seen that in all cases the noise levels decrease rapidly between 0.5 and 2.0 Hz, beyond which they generally continue to decrease at slower rates. Thus, the benefits associated with the improved stability of lower frequency data must be traded off against the general increase in noise level with decreasing frequency in the system design process. This is particularly true in cases where the smallest events of interest have magnitudes down near the detection thresholds of the seismic monitoring system. In such cases, data processed in bands below about 2 Hz will often not be recorded at useful signal-to-noise ratios.

Another factor to be considered in evaluating the results of Figure 19 is that there can be significant differences in the degree of difficulty of correcting for the effects of propagation on the various regional phase amplitudes. Thus, for example, although the  $\sigma_M$  values of Figure 19 indicate that the P wave data are least sensitive to propagation path variations for this sample of data, procedures for correcting for such effects are much more highly developed for the  $L_g$  phase than they are for the P phases. In this regard, it is worth noting from Figure 18 that the data recorded from the Lop Nor explosion at GARM provide  $S_n$  and  $L_g$  magnitude measures for that event which are significant outliers over much of the analyzed frequency band. Elimination of this one recording from the variance analysis leads to the revised  $\sigma_M$  results shown in

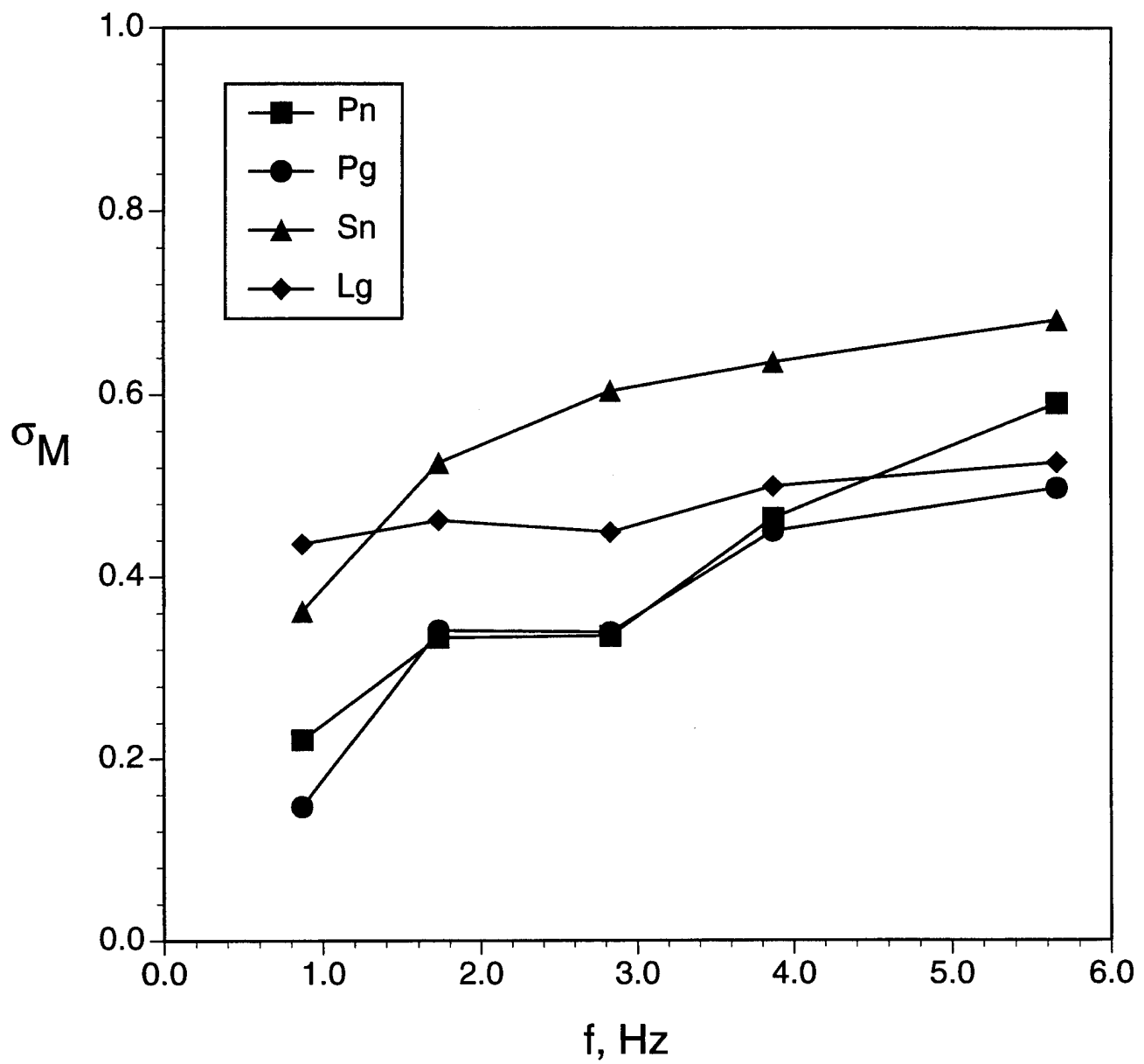


Figure 19. Standard deviation of the individual phase magnitudes as a function of frequency.

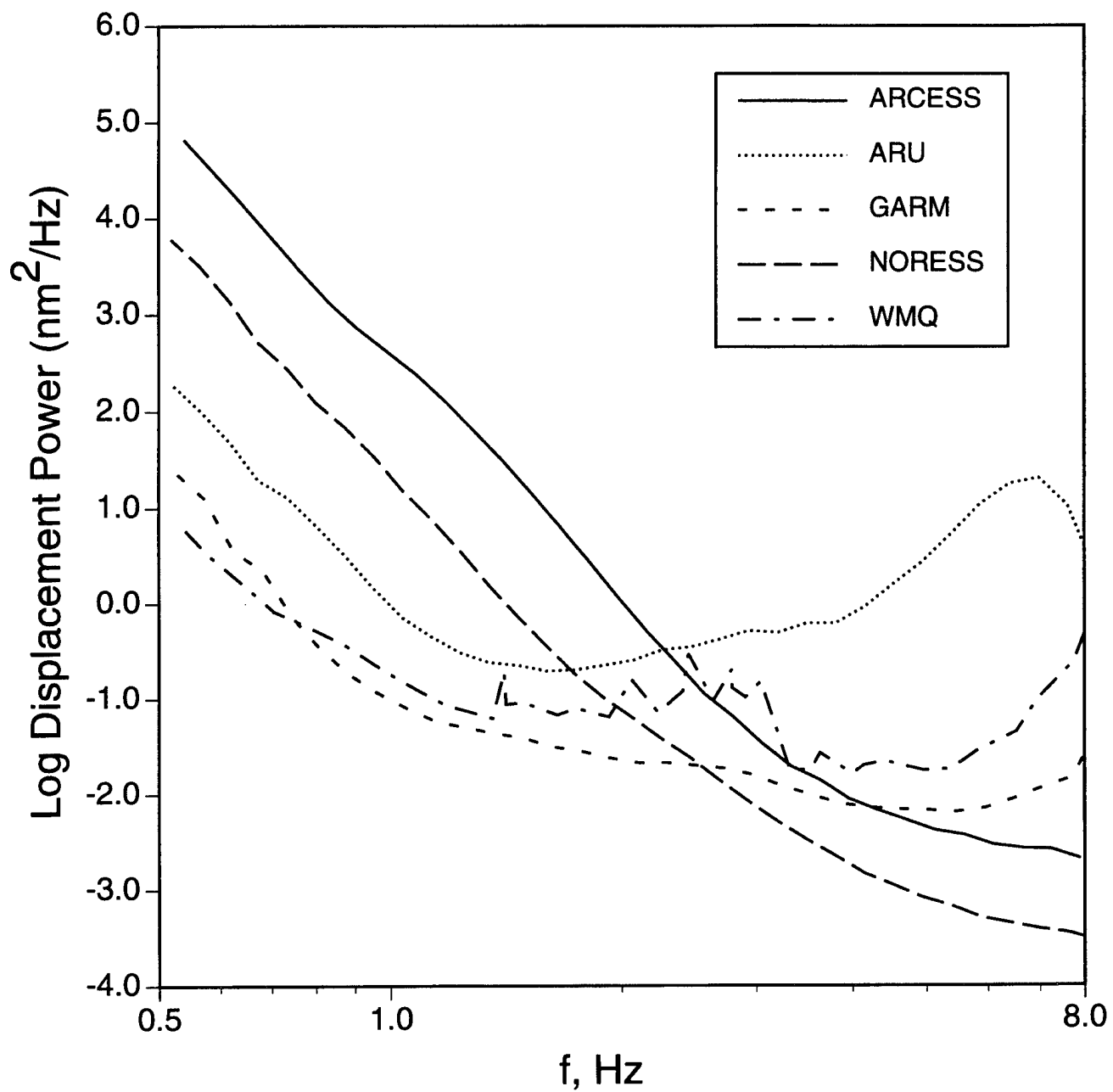


Figure 20. Average background noise levels as a function of frequency for the five selected regional stations.

Figure 21, where it can be seen that the  $L_g$  magnitude results are now very comparable to those obtained using the P phase data. Thus, if such variations in  $L_g$  propagation path effects can be reliably corrected using established procedures, there may be good reasons to prefer a magnitude measure based on that phase, particularly since such magnitudes have already been widely applied to both earthquake and nuclear explosion data. Additional research will be required in order to determine which of the available regional magnitude measures provides the best measure of source size for use in nuclear monitoring.

## 4. SUMMARY AND CONCLUSIONS

### 4.1 Summary

Given that the feasibility of the cavity decoupling evasion scenario has been experimentally confirmed, it follows that conclusive monitoring of any eventual CTBT will necessarily involve analyses of seismic signals recorded from small events with magnitudes approaching a threshold which is on the order of  $m_b = 2.0$  for evasively tested 1 kt nuclear explosions. However, the definition of meaningful magnitude measures for such small events remains as a major issue affecting assessments of seismic monitoring capability. That is, since such events are not expected to be detected teleseismically, their magnitudes will have to be estimated from regional distance recordings using seismic phases and frequency bands which are different from those employed in the teleseismic  $m_b$  scale which has traditionally been used to specify seismic monitoring capability. The investigations summarized in this report have centered on an attempt to quantitatively relate these different magnitude measures through analyses of synthetic regional seismic data corresponding to those to be expected from low yield cavity decoupled nuclear explosions at a variety of different test locations.

The problem of magnitude determination for small seismic events was reviewed in Section 2, where the magnitude ranges of potential interest in the seismic monitoring of underground nuclear testing were assessed and a variety of proposed regional magnitude measures were described and compared. In particular, the regional magnitude determination algorithm which has been

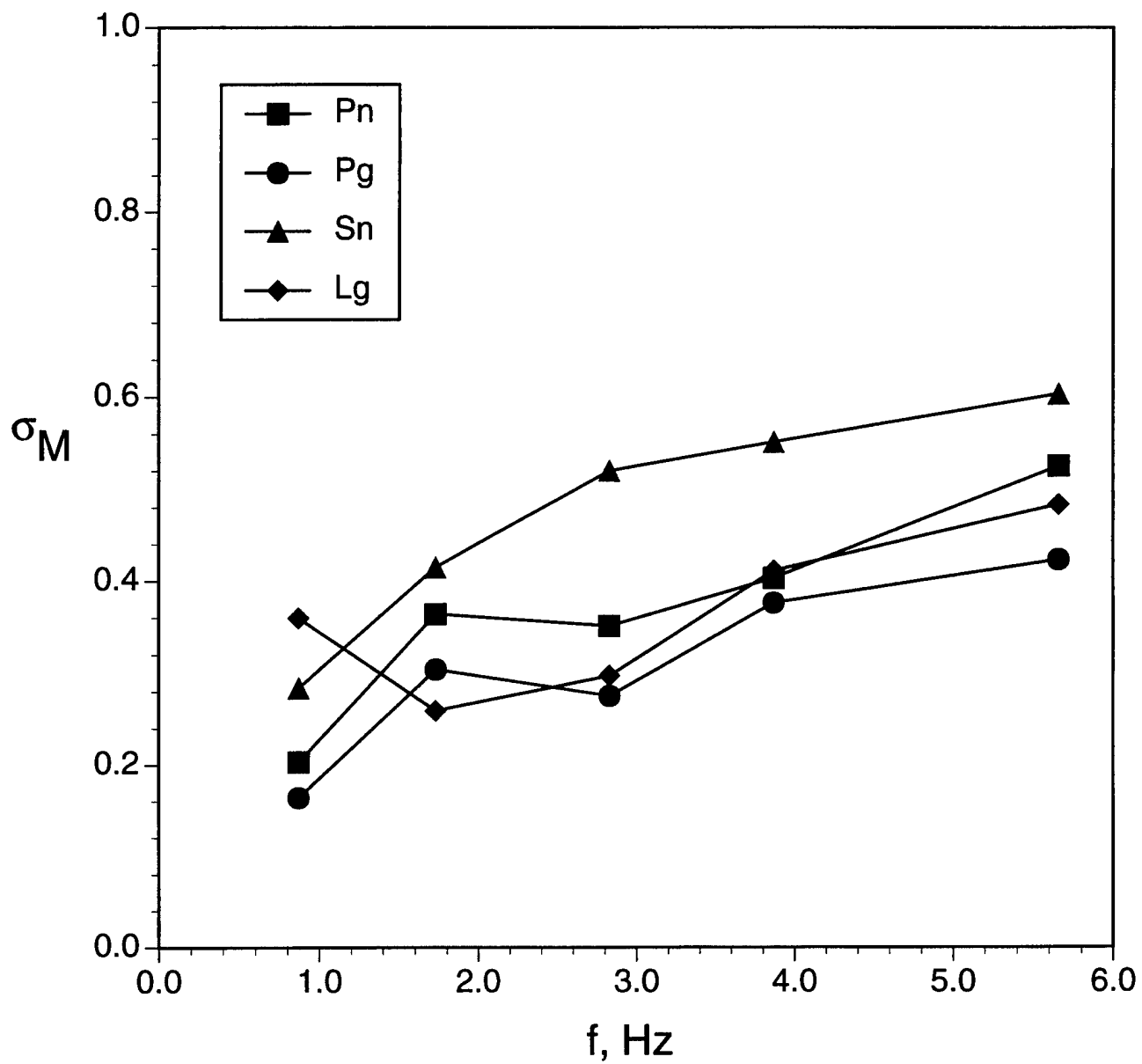


Figure 21. Modified estimates of the standard deviation of the individual phase magnitudes as a function of frequency.

implemented in the prototype International Monitoring System (IMS) running at the ARPA Center for Monitoring Research was reviewed; and it was concluded that it is quite different from most of the other  $M_L$  measures which have been proposed since Richter's original formulation of the seismic magnitude scale in that it incorporates data from the four distinct regional phases  $P_n$ ,  $P_g$ ,  $S_n$  and  $L_g$ .

The calibration of regional magnitude determinations for small nuclear explosions was considered in Section 3 using theoretically scaled regional seismic data corresponding to those to be expected from low yield cavity decoupled tests conducted at various source locations near Scandinavia and in Central Asia. Analyses of these synthetic data indicated that, even for well-calibrated stations such as the ARPA Scandinavian arrays, regional seismic magnitude measures can show pronounced dependence on variables such as source type and location. More specifically, it was demonstrated that differences between explosion and earthquake regional phase characteristics, such as the average  $L_g/P$  amplitude ratio, can lead to consistent biases between regional magnitude estimates for explosions and earthquakes having comparable  $m_b$  values. It follows that regional magnitude algorithms which have been calibrated using earthquake and mine blast data will not be directly applicable to nuclear explosion data, and this fact will need to be considered in any assessments of the capabilities of proposed seismic networks for use in CTBT monitoring.

## 4.2 Conclusions

The research summarized above supports the following general conclusions regarding the calibration of local magnitude scales for use in seismic monitoring.

- (1) Comprehensive seismic monitoring of underground nuclear testing in the 1 to 10 kt range will necessarily involve analyses of small seismic events with magnitudes in the range  $2.0 < m_b < 3.5$ , at least in regions where cavity decoupling is considered to be feasible over this yield range.
- (2) The wide variety of regional magnitude scales which have been proposed to measure source size are based on a multitude of different seismic phases and encompass a wide range of dominant frequencies; and,



consequently, they can not be simply related to the teleseismic  $m_b$  scale which has traditionally been used to specify seismic monitoring capability.

(3) Even for extensively calibrated stations such as the ARPA Scandinavian arrays, significant magnitude biases can occur for events with epicenters in areas which are not well represented in the calibration databases.

(4) Regional magnitude determination algorithms which have been calibrated using earthquake and mine blast data can be expected to underestimate the sizes of small nuclear explosions due to the systematic differences in relative phase excitation levels (e.g.,  $L_g/P$ ) associated with the different source types.

(5) Addition of new stations to a regional monitoring network will generally require the collection and detailed analysis of large, representative calibration databases before such stations can be expected to contribute meaningful data for use in the determination of regional magnitudes.

(6) The variance of the regional phase amplitude data analyzed in this study increases with increasing frequency above 1 Hz and is smaller for P than for S phases. However, complications associated with the frequency dependent nature of the seismic background noise and calibration issues also need to be considered in selecting a regional magnitude measure for use in seismic monitoring.

## REFERENCES

- Bache, T. C., S. R. Bratt, J. W. Given, T. D. Schroeder, H. J. Swanger, and J. Wang (1991), The Intelligent Monitoring System Version 2, NMRD Quarterly Technical Report #7, October 1991, SAIC Report, San Diego.
- Båth, M., O. Kulháněk, T. Van Eck, and R. Wahlström (1976), Engineering Analysis of Ground Motion in Sweden, Swedish Seismological Institute Report 5-76.
- Gutenberg, B. (1945a), "Amplitudes of Surface Waves and Magnitudes of Shallow Earthquakes," *Bull. Seism. Soc. Am.*, 35, pp.3-12.
- Gutenberg, B. (1945b), "Amplitudes of P, PP and S and Magnitudes of Shallow Earthquakes," *Bull. Seism. Soc. Am.*, 35, pp.57-69.
- Mueller, R. A. and J. R. Murphy (1971), "Seismic Characteristics of Underground Nuclear Detonations. Part I. Seismic Spectrum Scaling," *Bull. Seism. Soc. Am.*, 61, 1975.
- Murphy, J. R. (1977), "Seismic Source Functions and Magnitude Determinations for Underground Nuclear Detonations," *Bull. Seism. Soc. Am.*, 67, 135-158.
- Murphy, J. R. and B. W. Barker (1994), "Seismic Identification Analyses of Cavity Decoupled Nuclear and Chemical Explosions," S-CUBED Technical Report SSS-TR-94-14399 (PL-TR-94-2036), ADA280947.
- Mykkeltveit, S., and H. Bungum (1984), "Processing of Regional Seismic Events Using Data from Small Aperture Arrays," *Bull. Seism. Soc. Am.*, 74, pp. 2213-2333.
- Nuttli, O. W. (1973), "Seismic Wave Attenuation and Magnitude Relations for Eastern North America," *J. Geophys. Res.*, 78, pp. 876-885.
- Richter, C. F. (1935), "An Instrumental Earthquake Magnitude Scale," *Bull. Seism. Soc. Am.*, 25, pp. 1-32.
- Ringdal, F. (1983), "Magnitudes from P Coda and L<sub>g</sub> Using NORSAR Data," in NORSAR Semiannual Technical Summary, 1 October 82 - 31 March 1983, NORSAR Scientific Report 2-82/83.

Ringdal, F., and J. Fyen (1991), "RMS  $L_g$  Analysis of Novaya Zemlya Explosion Recordings," in NORSAR Semiannual Technical Summary, 1 October 90 - 31 March 1991, NORSAR Scientific Report 2-90/91, pp. 53-67.

Sereno, T. J., and S. R. Bratt (1988), Attenuation and Detection Capability of Regional Phases Recorded at NORESS, AFGL Report AFGL-TR-88-0095, ADA196568.

Prof. Thomas Ahrens  
Seismological Lab, 252-21  
Division of Geological & Planetary Sciences  
California Institute of Technology  
Pasadena, CA 91125

Prof. Keiiti Aki  
Center for Earth Sciences  
University of Southern California  
University Park  
Los Angeles, CA 90089-0741

Prof. Shelton Alexander  
Geosciences Department  
403 Deike Building  
The Pennsylvania State University  
University Park, PA 16802

Prof. Charles B. Archambeau  
University of Colorado  
JSPC  
Campus Box 583  
Boulder, CO 80309

Dr. Thomas C. Bache, Jr.  
Science Applications Int'l Corp.  
10260 Campus Point Drive  
San Diego, CA 92121 (2 copies)

Prof. Muawia Barazangi  
Cornell University  
Institute for the Study of the Continent  
3126 SNEE Hall  
Ithaca, NY 14853

Dr. Jeff Barker  
Department of Geological Sciences  
State University of New York  
at Binghamton  
Vestal, NY 13901

Dr. Douglas R. Baumgardt  
ENSCO, Inc  
5400 Port Royal Road  
Springfield, VA 22151-2388

Dr. Susan Beck  
Department of Geosciences  
Building #77  
University of Arizona  
Tucson, AZ 85721

Dr. T.J. Bennett  
S-CUBED  
A Division of Maxwell Laboratories  
11800 Sunrise Valley Drive, Suite 1212  
Reston, VA 22091

Dr. Robert Blandford  
AFTAC/TT, Center for Seismic Studies  
1300 North 17th Street  
Suite 1450  
Arlington, VA 22209-2308

Dr. Stephen Bratt  
ARPA/NMRO  
3701 North Fairfax Drive  
Arlington, VA 22203-1714

Dale Breeding  
U.S. Department of Energy  
Recipient, IS-20, GA-033  
Office of Arms Control  
Washington, DC 20585

Dr. Lawrence Burdick  
C/O Barbara Wold  
Dept of Biology  
CA Inst. of Technology  
Pasadena, CA 91125

Dr. Robert Burrridge  
Schlumberger-Doll Research Center  
Old Quarry Road  
Ridgefield, CT 06877

Dr. Jerry Carter  
Center for Seismic Studies  
1300 North 17th Street  
Suite 1450  
Arlington, VA 22209-2308

Dr. Martin Chapman  
Department of Geological Sciences  
Virginia Polytechnical Institute  
21044 Derring Hall  
Blacksburg, VA 24061

Mr Robert Cockerham  
Arms Control & Disarmament Agency  
320 21st Street North West  
Room 5741  
Washington, DC 20451,

Prof. Vernon F. Cormier  
Department of Geology & Geophysics  
U-45, Room 207  
University of Connecticut  
Storrs, CT 06268

Prof. Steven Day  
Department of Geological Sciences  
San Diego State University  
San Diego, CA 92182

Dr. Zoltan Der  
ENSCO, Inc.  
5400 Port Royal Road  
Springfield, VA 22151-2388

Dr. Stanley K. Dickinson  
AFOSR/NM  
110 Duncan Avenue  
Suite B115  
Bolling AFB, DC 20332-6448

Prof. Adam Dziewonski  
Hoffman Laboratory, Harvard University  
Dept. of Earth Atmos. & Planetary Sciences  
20 Oxford Street  
Cambridge, MA 02138

Prof. John Ebel  
Department of Geology & Geophysics  
Boston College  
Chestnut Hill, MA 02167

Dr. Petr Firbas  
Institute of Physics of the Earth  
Masaryk University Brno  
Jecna 29a  
612 46 Brno, Czech Republic

Dr. Mark D. Fisk  
Mission Research Corporation  
735 State Street  
P.O. Drawer 719  
Santa Barbara, CA 93102

Prof. Donald Forsyth  
Department of Geological Sciences  
Brown University  
Providence, RI 02912

Dr. Cliff Frolich  
Institute of Geophysics  
8701 North Mopac  
Austin, TX 78759

Dr. Holly Given  
IGPP, A-025  
Scripps Institute of Oceanography  
University of California, San Diego  
La Jolla, CA 92093

Dr. Jeffrey W. Given  
SAIC  
10260 Campus Point Drive  
San Diego, CA 92121

Dr. Indra N. Gupta  
Multimax, Inc.  
1441 McCormick Drive  
Landover, MD 20785

Dan N. Hagedon  
Pacific Northwest Laboratories  
Battelle Boulevard  
Richland, WA 99352

Dr. James Hannon  
Lawrence Livermore National Laboratory  
P.O. Box 808, L-205  
Livermore, CA 94550

Prof. Danny Harvey  
University of Colorado, JSPC  
Campus Box 583  
Boulder, CO 80309

Prof. Donald V. Helmberger  
Division of Geological & Planetary Sciences  
California Institute of Technology  
Pasadena, CA 91125

Prof. Eugene Herrin  
Geophysical Laboratory  
Southern Methodist University  
Dallas, TX 75275

Prof. Robert B. Herrmann  
Department of Earth & Atmospheric Sciences  
St. Louis University  
St. Louis, MO 63156

Prof. Lane R. Johnson  
Seismographic Station  
University of California  
Berkeley, CA 94720

Prof. Thomas H. Jordan  
Department of Earth, Atmospheric &  
Planetary Sciences  
Massachusetts Institute of Technology  
Cambridge, MA 02139

Prof. Alan Kafka  
Department of Geology & Geophysics  
Boston College  
Chestnut Hill, MA 02167

U.S. Dept of Energy  
Max Koontz, NN-20, GA-033  
Office of Research and Develop.  
1000 Independence Avenue  
Washington, DC 20585

Dr. Richard LaCoss  
MIT Lincoln Laboratory, M-200B  
P.O. Box 73  
Lexington, MA 02173-0073

Dr. Fred K. Lamb  
University of Illinois at Urbana-Champaign  
Department of Physics  
1110 West Green Street  
Urbana, IL 61801

Prof. Charles A. Langston  
Geosciences Department  
403 Deike Building  
The Pennsylvania State University  
University Park, PA 16802

Jim Lawson, Chief Geophysicist  
Oklahoma Geological Survey  
Oklahoma Geophysical Observatory  
P.O. Box 8  
Leonard, OK 74043-0008

Prof. Thorne Lay  
Institute of Tectonics  
Earth Science Board  
University of California, Santa Cruz  
Santa Cruz, CA 95064

Dr. William Leith  
U.S. Geological Survey  
Mail Stop 928  
Reston, VA 22092

Mr. James F. Lewkowicz  
Phillips Laboratory/GPE  
29 Randolph Road  
Hanscom AFB, MA 01731-3010( 2 copies)

Prof. L. Timothy Long  
School of Geophysical Sciences  
Georgia Institute of Technology  
Atlanta, GA 30332

Dr. Randolph Martin, III  
New England Research, Inc.  
76 Olcott Drive  
White River Junction, VT 05001

Dr. Robert Masse  
Denver Federal Building  
Box 25046, Mail Stop 967  
Denver, CO 80225

Dr. Gary McCartor  
Department of Physics  
Southern Methodist University  
Dallas, TX 75275

Prof. Thomas V. McEvilly  
Seismographic Station  
University of California  
Berkeley, CA 94720

Dr. Art McGarr  
U.S. Geological Survey  
Mail Stop 977  
U.S. Geological Survey  
Menlo Park, CA 94025

Dr. Keith L. McLaughlin  
S-CUBED  
A Division of Maxwell Laboratory  
P.O. Box 1620  
La Jolla, CA 92038-1620

Stephen Miller & Dr. Alexander Florence  
SRI International  
333 Ravenswood Avenue  
Box AF 116  
Menlo Park, CA 94025-3493

Prof. Bernard Minster  
IGPP, A-025  
Scripps Institute of Oceanography  
University of California, San Diego  
La Jolla, CA 92093

Prof. Brian J. Mitchell  
Department of Earth & Atmospheric Sciences  
St. Louis University  
St. Louis, MO 63156

Mr. Richard J. Morrow  
USACDA/IVI  
320 21st St. N.W.  
Washington, DC 20451

Mr. Jack Murphy  
S-CUBED  
A Division of Maxwell Laboratory  
11800 Sunrise Valley Drive, Suite 1212  
Reston, VA 22091 (2 Copies)

Dr. Keith K. Nakanishi  
Lawrence Livermore National Laboratory  
L-025  
P.O. Box 808  
Livermore, CA 94550

Prof. John A. Orcutt  
IGPP, A-025  
Scripps Institute of Oceanography  
University of California, San Diego  
La Jolla, CA 92093

Prof. Jeffrey Park  
Kline Geology Laboratory  
P.O. Box 6666  
New Haven, CT 06511-8130

Dr. Howard Patton  
Lawrence Livermore National Laboratory  
L-025  
P.O. Box 808  
Livermore, CA 94550

Dr. Frank Pilotte  
HQ AFTAC/TT  
1030 South Highway A1A  
Patrick AFB, FL 32925-3002

Dr. Jay J. Pulli  
Radix Systems, Inc.  
6 Taft Court  
Rockville, MD 20850

Dr. Robert Reinke  
ATTN: FCTVTD  
Field Command  
Defense Nuclear Agency  
Kirtland AFB, NM 87115

Prof. Paul G. Richards  
Lamont-Doherty Earth Observatory  
of Columbia University  
Palisades, NY 10964

Mr. Wilmer Rivers  
Teledyne Geotech  
1300 17th St N #1450  
Arlington, VA 22209-3803

Dr. Alan S. Ryall, Jr.  
Lawrence Livermore National Laboratory  
P.O. Box 808, L-205  
Livermore, CA 94550

Dr. Chandan K. Saikia  
Woodward Clyde- Consultants  
566 El Dorado Street  
Pasadena, CA 91101

Dr. Richard Sailor  
TASC, Inc.  
55 Walkers Brook Drive  
Reading, MA 01867

Prof. Charles G. Sammis  
Center for Earth Sciences  
University of Southern California  
University Park  
Los Angeles, CA 90089-0741

Prof. Christopher H. Scholz  
Lamont-Doherty Earth Observatory  
of Columbia University  
Palisades, NY 10964

Dr. Susan Schwartz  
Institute of Tectonics  
1156 High Street  
Santa Cruz, CA 95064

Mr. Dogan Seber  
Cornell University  
Inst. for the Study of the Continent  
3130 SNEE Hall  
Ithaca, NY 14853-1504

Secretary of the Air Force  
(SAFRD)  
Washington, DC 20330

Office of the Secretary of Defense  
DDR&E  
Washington, DC 20330

Thomas J. Sereno, Jr.  
Science Application Int'l Corp.  
10260 Campus Point Drive  
San Diego, CA 92121

Dr. Michael Shore  
Defense Nuclear Agency/SPSS  
6801 Telegraph Road  
Alexandria, VA 22310

Dr. Robert Shumway  
University of California Davis  
Division of Statistics  
Davis, CA 95616

Dr. Matthew Sibol  
Virginia Tech  
Seismological Observatory  
4044 Derring Hall  
Blacksburg, VA 24061-0420

Prof. David G. Simpson  
IRIS, Inc.  
1616 North Fort Myer Drive  
Suite 1050  
Arlington, VA 22209

Donald L. Springer  
Lawrence Livermore National Laboratory  
L-025  
P.O. Box 808  
Livermore, CA 94550

Dr. Jeffrey Stevens  
S-CUBED  
A Division of Maxwell Laboratory  
P.O. Box 1620  
La Jolla, CA 92038-1620

Prof. Brian Stump  
Los Alamos National Laboratory  
EES-3  
Mail Stop C-335  
Los Alamos, NM 87545

Prof. Jeremiah Sullivan  
University of Illinois at Urbana-Champaign  
Department of Physics  
1110 West Green Street  
Urbana, IL 61801

Prof. L. Sykes  
Lamont-Doherty Earth Observatory  
of Columbia University  
Palisades, NY 10964

Dr. Steven R. Taylor  
Los Alamos National Laboratory  
P.O. Box 1663  
Mail Stop C335  
Los Alamos, NM 87545

Prof. Tuncay Taymaz  
Istanbul Technical University  
Dept. of Geophysical Engineering  
Mining Faculty  
Maslak-80626, Istanbul Turkey

Prof. Clifford Thurber  
University of Wisconsin-Madison  
Department of Geology & Geophysics  
1215 West Dayton Street  
Madison, WS 53706

Prof. M. Nafi Toksoz  
Earth Resources Lab  
Massachusetts Institute of Technology  
42 Carleton Street  
Cambridge, MA 02142

Dr. Larry Turnbull  
CIA-OSWR/NED  
Washington, DC 20505

Dr. Gregory van der Vink  
IRIS, Inc.  
1616 North Fort Myer Drive  
Suite 1050  
Arlington, VA 22209

Dr. Karl Veith  
EG&G  
2341 Jefferson Davis Highway  
Suite 801  
Arlington, VA 22202-3809

Prof. Terry C. Wallace  
Department of Geosciences  
Building #77  
University of Arizona  
Tuscon, AZ 85721

Dr. Thomas Weaver  
Los Alamos National Laboratory  
P.O. Box 1663  
Mail Stop C335  
Los Alamos, NM 87545

Dr. William Wortman  
Mission Research Corporation  
8560 Cinderbed Road  
Suite 700  
Newington, VA 22122

Prof. Francis T. Wu  
Department of Geological Sciences  
State University of New York  
at Binghamton  
Vestal, NY 13901

Prof Ru-Shan Wu  
University of California, Santa Cruz  
Earth Sciences Department  
Santa Cruz, CA 95064



ARPA, OASB/Library  
3701 North Fairfax Drive  
Arlington, VA 22203-1714

HQ DNA  
ATTN: Technical Library  
Washington, DC 20305

Defense Technical Information Center  
8725 John J. Kingman Road  
Ft Belvoir, VA 22060-6218(2 copies)

TACTEC  
Battelle Memorial Institute  
505 King Avenue  
Columbus, OH 43201 (Final Report)

Phillips Laboratory  
ATTN: XPG  
29 Randolph Road  
Hanscom AFB, MA 01731-3010

Phillips Laboratory  
ATTN: GPE  
29 Randolph Road  
Hanscom AFB, MA 01731-3010

Phillips Laboratory  
ATTN: TSML  
5 Wright Street  
Hanscom AFB, MA 01731-3004

Phillips Laboratory  
ATTN: PL/SUL  
3550 Aberdeen Ave SE  
Kirtland, NM 87117-5776 (2 copies)

Dr. Michel Bouchon  
I.R.I.G.M.-B.P. 68  
38402 St. Martin D'Herès  
Cedex, FRANCE

Dr. Michel Campillo  
Observatoire de Grenoble  
I.R.I.G.M.-B.P. 53  
38041 Grenoble, FRANCE

Prof. Hans-Peter Harjes  
Institute for Geophysics  
Ruhr University/Bochum  
P.O. Box 102148  
4630 Bochum 1, GERMANY

Prof. Eystein Husebye  
IFJF  
Jordskjelvstasjonen  
Allegaten, 5007 BERGEN NORWAY

David Jepsen  
Acting Head, Nuclear Monitoring Section  
Bureau of Mineral Resources  
Geology and Geophysics  
G.P.O. Box 378, Canberra, AUSTRALIA

Ms. Eva Johannisson  
Senior Research Officer  
FOA  
S-172 90 Sundbyberg, SWEDEN

Dr. Peter Marshall  
Procurement Executive  
Ministry of Defense  
Blacknest, Brimpton  
Reading FG7-FRS, UNITED KINGDOM

Dr. Bernard Massinon, Dr. Pierre Mechler  
Société Radiomana  
27 rue Claude Bernard  
75005 Paris, FRANCE (2 Copies)

Dr. Svein Mykkeltveit  
NTNT/NORSAR  
P.O. Box 51  
N-2007 Kjeller, NORWAY (3 Copies)

Prof. Keith Priestley  
University of Cambridge  
Bullard Labs, Dept. of Earth Sciences  
Madingley Rise, Madingley Road  
Cambridge CB3 0EZ, ENGLAND

Dr. Jorg Schlittenhardt  
Federal Institute for Geosciences & Nat'l Res.  
Postfach 510153  
D-30631 Hannover, GERMANY

Dr. Johannes Schweitzer  
Institute of Geophysics  
Ruhr University/Bochum  
P.O. Box 1102148  
4360 Bochum 1, GERMANY

Trust & Verify  
VERTIC  
Carrara House  
20 Embankment Place  
London WC2N 6NN, ENGLAND

Prof. Dr. M. Namik YALCIN  
Dept. of Earth Sciences  
P.O. Box 21,  
41470  
GEBZE-KOCAELI, TURKEY